Collagen XIII-derived ectodomain regulates bone angiogenesis and intracortical remodeling

Jarkko Koivunen, Antti V. Kemppainen, Mikko A. Finnilä, Riikka Keski-Filppula, Heli Härönen, Hongmin Tu, Henri Pellikka, Anne Heikkinen, Elina Kylmäoja, Raija Sormunen, Ilkka Miinalainen, Simo Saarakkala, Valerio Izzi, Taina Pihlajaniemi

PII: S0945-053X(19)30159-3
DOI: https://doi.org/10.1016/j.matbio.2019.06.005
Reference: MATBIO 1573

To appear in: *Matrix Biology*

Received date: 4 April 2019
Revised date: 12 June 2019
Accepted date: 12 June 2019

Please cite this article as: J. Koivunen, A.V. Kemppainen, M.A. Finnilä, et al., Collagen XIII-derived ectodomain regulates bone angiogenesis and intracortical remodeling, Matrix Biology, https://doi.org/10.1016/j.matbio.2019.06.005

Collagen XIII-derived ectodomain regulates bone angiogenesis and intracortical remodeling

Jarkko Koivunen[1,5,6], Antti V. Kemppainen[1], Mikko A. Finnilä[2], Riikka Keski-Filppula[1], Heli Härönen[1], Hongmin Tu[1], Henri Pellikka[1], Anne Heikkinen[1], Elina Kylmäoja[3], Raija Sormunen[4], Ilkka Miinalainen[4], Simo Saarakkala[2], Valerio Izzi[1], Taina Pihlajaniemi[1,5]

[1]Oulu Center for Cell-Matrix Research and Biocenter Oulu, Faculty of Biochemistry and Molecular Medicine, P.O. Box 5400, FIN-90014 University of Oulu, Oulu, Finland

[2]Department of Medical Technology, Institute of Biomedicine, University of Oulu, P.O. Box 5000, FIN-90014 University of Oulu, Oulu, Finland

[3]Institute of Cancer Research and Translational Medicine, Department of Anatomy and Cell Biology, Medical Research Center, P.O. Box 5400, FIN-90014 University of Oulu, Oulu, Finland

[4]Biocenter Oulu, P.O. Box 5000, FIN-90014 University of Oulu, Oulu, Finland

[5]Corresponding author

[6]Lead contact: jarkko.koivunen@oulu.fi

Abstract

Osteoporosis is the most common degenerative bone disease that occurs when the balance of bone production and resorption is perturbed. Loss of bone mass or alteration in its quality leads to significant weakening of the bones and subsequently to higher fracture risk. Collagen XIII (ColXIII) is a conserved transmembrane protein expressed in many mesenchymal tissues. Here we show that ColXIII is a regulator of bone remodeling niche. In this study, we found that ColXIII expression is significantly upregulated in osteoporotic patients. In view of that, we studied bone homeostasis in ColXIII-overexpressing mice (*Col13a1*^{oe}) up to 72 weeks of age and observed a cortical bone overgrowth followed by a drastic bone loss, together with increased bone vascularization. Moreover, our results demonstrate that the ColXIII-derived ectodomain enhances angiogenesis through β1-integrins and the JNK pathway. Consequently, these data suggest that ColXIII has a role in age-dependent cortical bone deterioration with possible implications for osteoporosis and fracture risk.

Keywords: Bone matrix, Bone remodeling, Molecular pathways, Osteoblasts, Osteoclasts

Introduction

Bone homeostasis is a complex multicellular process orchestrated by multiple paracrine and endocrine signals produced mainly by bone-specific cell types such as osteoblasts, bone forming cells, and osteoclasts that resorb mineralized bone [1-3]. In part, because they synthesize and secrete collagen molecules, osteoblasts play an important role in regulating bone homeostasis. Eventually, some osteoblasts are embedded in the bone matrix and differentiate to osteocytes, which act as mechanosensory cells and significantly contribute to bone homeostasis [4]. Clinically, the most common bone disease is osteoporosis, a growing public health concern affecting millions of people [5,6], characterized by bone loss and the reduction of bone mineral density, and the subsequent decrease of bone strength leads to a severe increase in the risk of fractures [5,6].

Collagens are fundamental structural components of all connective tissues and have the ability to modulate cell signaling, both during development and postnatally. Collagen XIII (ColXIII) is a type II transmembrane protein belonging to the subgroup of membrane-associated collagens with interrupted triple-helices (MACITs)[7,8] which is known to interact with other molecules such as fibronectin, heparin, the basement membrane components nidogen-2 and perlecan, and $\alpha 1\beta 1$ integrin [9,10]. Structurally, ColXIII contains a short cytosolic domain, a transmembrane domain, and a longer rod-like ectodomain that is about 150 nm in length [10]. The ectodomain of ColXIII can be shed from the plasma membrane by furin-mediated cleavage to produce a soluble ectodomain [11,12], and previous studies indicate that transmembrane and shed forms of ColXIII may have distinct functions [13-15].

ColXIII is expressed in many tissues, such as bone, cartilage, heart, muscle and skin throughout development and adult life [16,17]. In particular, the neuromuscular junction, the periosteum, mesenchymal stem cells (MSCs) and mature osteoblasts show high expression of ColXIII [18-21]. Additionally, it has been shown that loss-of-function mutations in the human *COL13A1* gene lead to congenital myasthenic syndrome type 19, a disease that includes skeletal abnormalities, such as micrognathia, pes cavus, and pigeon chest [22]. Moreover, a recent study revealed that ColXIII promotes breast cancer progression and metastasis [23]. However, ColXIII-related pathways and mechanisms of action are not well understood.

Genetically modified mouse models have suggested that ColXIII affects bone development [19] and contributes to microvessel development [24]. We have previously generated a transgenic mouse line overexpressing ColXIII α1 chains (*Col13a1*^{oe})[19]. This line showed robust expression of the transgene in skeletal tissues, the expression pattern mimicking that of endogenous ColXIII, and, more interestingly, we found that ColXIII overexpression caused an increase in bone mass [19]. In the present study, by combining bioinformatics analysis of human mesenchymal cells with *in vivo* and *in vitro* studies, we discovered a prominent role for ColXIII in osteogenesis, bone angiogenesis, and intracortical remodeling.

Results

COL13A1 is linked to osteoporosis

In order to study the role of ColXIII in osteogenesis, we first analyzed microarray data of human mesenchymal stem cells (hMSCs) downloaded from Gene Expression Omnibus (GEO)[21]. Data were obtained from healthy middle-aged (42–67 years old), healthy elderly (79–89 years old), elderly osteoporotic donors (79–94 years old), and long term-cultivated *in vitro* senescent hMSCs. Interestingly, we observed a 2.5-fold upregulation of *COL13A1* in osteoporotic patients compared with age-matched healthy donors (Fig. 1A). Notably, *COL13A1* expression was significantly upregulated in the elderly osteoporotic group when compared to middle-aged, healthy elderly or senescent hMSCs, demonstrating that *COL13A1* is linked to osteoporosis, not to normal aging or cell senescence. Furthermore, we found that *COL13A1* expression correlates linearly with genes associated with bone mineral density (BMD) or fracture risk such as *COL1A1* (Fig. 1B), *RUNX2* (Fig. 1C), and *VEGF* (Fig. 1D), while a correlation was not detected between *COL13A1* and *JAGGED1* (an osteoporosis-related NOTCH ligand)[21] (Fig. 1E) or *SOST* (a negative regulator of bone growth)[25](Fig. 1F). Since these data suggest a possible association between increased ColXIII expression and osteoporosis, we proceeded to study bone development and homeostasis in *Col13a1*^{oe} mice from 4 to 72 weeks of age.

Col13a1^{oe} mice possess a cortical bone overgrowth followed by drastic endocortical bone loss

The femoral cortical and trabecular bone morphology of *Col13a1*^{oe} mice was evaluated in both genders at five time points by micro-computed tomography (μCT). For each set of *Col13a1*^{oe} mice, a wild type (WT) control group of littermates was assessed, with a total of 4-7 mice per group. *Col13a1*^{oe} mice of either gender had significantly shorter femurs than their WT littermates at the 4-week time point, but

no major differences were observed at later time points (Fig. S1A). Moreover, we observed a high bone mass phenotype that was restricted to the diaphyseal region (Fig. 2A and S2). Already at 4 weeks of age, the *Col13a1*^{oe} mice had a visibly thickened mid-diaphysis compared with WT mice, and subsequently the *Col13a1*^{oe} bone area and perimeter were grossly increased at all studied time points from 12 to 72 weeks of age (Fig. 2A). The substantial increase in bone volume was followed by massive bone loss from the endosteal surface from 35 weeks onwards, creating cortical remnants inside the bone marrow cavity (Fig. 2A). More specifically, the femoral cortical bone phenotype of male *Col13a1*^{oe} mice became evident at the age of 4 weeks, and the difference gradually increased, reaching its peak at 25 weeks when the femoral cortical bone area (Ct.Ar) was increased by 17-fold (Fig. 2B), the medullary area (Ma.Ar) by 8.4-fold (Fig. 2C), and the cortical thickness (Ct.Th) by 1.7-fold (Fig. 2D) compared to WT mice. At 72 weeks of age, the *Col13a1*^{oe} Ct.Ar remained 10-fold and the Ma.Ar 11-fold higher than in WT mice, whereas the Ct.Th was significantly thinner than in WT mice. Comparable results were observed in female *Col13a1*^{oe} mice (Fig. 2B-D), and, altogether, these μCT results support the notion that ColXIII has an association with cortical bone loss.

We also analyzed trabecular bone morphology in both genders by μCT (Fig. 3A-B and S3). At 4 weeks of age, the femoral trabecular bone fraction (BV/TV, Fig. 3C) and the trabecular number (Tb.N, Fig. 3D) were lower in both genders of *Col13a1*^{oe} mice compared to controls, though these differences were diminished over the period from 12 to 35 weeks. At 72 weeks of age, Tb.N, was higher in the *Col13a1*^{oe} males compared to WT littermates. The *Col13a1*^{oe} females showed similar developments, although they had higher BV/TV and Tb.N compared to WT already at 25 weeks, and the difference gradually increased toward 72 weeks of age, when the mutant BV/TV and Tb.N were almost 2-fold higher compared to WT. It should be noted that the total region of interest (TV) and trabecular bone volume (BV) were significantly higher in the *Col13a1*^{oe} mice in both genders from the 12- to the 72-

week time points compared to WT controls (Fig. S4A-B). We also performed histomorphometric analysis of WT and *Col13a1*^{oe} mice vertebrae trabecular bone but no statistical significance was observed (Fig. S4C-E).

Col13a1^{oe} mice have altered bone composition

Next, we studied the bone composition in detail by carrying out X-ray photoelectron spectroscopy (XPS) studies of cortical bone. XPS, also called electron spectroscopy for chemical analysis (ESCA), is a semi-quantitative chemical surface analysis method based on the X-ray-induced photoemission that provides information about the chemical composition of the sample [26,27]. We measured carbon, calcium, nitrogen, oxygen, and phosphorus content in the midshaft cross sections of *Col13a1*^{oe} and WT femurs and found that, in both 4- and 25-week-old *Col13a1*^{oe} mice, the femurs had significantly less calcium (Fig. 4A) and more nitrogen (Fig. 4B) than the WT littermates. We did not observe gender-specific variations in the bone composition at 25 weeks of age (Fig. S5A-B). The carbon content was significantly higher in 25-week-old *Col13a1*^{oe} mice compared to WT (Fig. S5C), whereas oxygen and phosphorus were significantly lower in the *Col13a1*^{oe} mice (Fig. S5D-E).

Subsequently, we addressed the quantity and orientation of fibrillar collagens of cortical bone by second harmonic generation (SHG) microscopy [28,29]. SHG is based on the highly non-centrosymmetric character of collagen molecules, which produces bright SHG signals reflecting the amount of collagen content in the tissue sample [28,29]. We analyzed non-stained, undecalcified cortical bone of 12-week-old mice tibias by using SHG microscopy and detected brighter SHG signal in *Col13a1*^{oe} tibias compared to controls indicating higher collagen I (ColI) content (Fig. 4C and D). Additionally, in the *Col13a1*^{oe} femoral cortical bone, the ColI fibrils were disorganized, whereas in WT

mice such fibrils were aligned in parallel (Fig. 4C and D). Hence, XPS and SHG data supported each other and showed that overexpression of ColXIII had major effects on both bone composition and organization.

Col13a1^{oe} mice have a poorly developed lacuno-canalicular network in long bones

As the μCT images of the *Col13a1^{oe}* bones indicated high cortical porosity and abnormal morphology, we studied the architecture of the lacunar-canalicular network in the *Col13a1^{oe}* and WT mice by SEM. SEM imaging of the bone revealed that the *Col13a1^{oe}* lacuno-canalicular network does not differentiate properly and remains significantly underdeveloped (Fig. 4E-H). These findings were confirmed by confocal imaging using femurs embedded in rhodamine 6G containing poly(methyl methacrylate) (PMMA)[30]. In agreement with the SEM results, confocal imaging revealed that *Col13a1^{oe}* bones had less canaliculi and that the lacunas were rounder and not linearly aligned as they were in WT (Fig. 4I-L). The changes in the lacuna-canalicular network of *Col13a1^{oe}* mice persist during aging (Fig. S6A-D). Moreover, the rhodamine and immunofluorescence (IF) staining revealed higher number of blood vessels inside the *Col13a1^{oe}* cortical bone compared with WT samples (Fig. 4K-L, Fig. S6E-F), and immunohistochemical (IHC) staining proposed enhanced VEGF expression in the *Col13a1^{oe}* mouse tibias (Fig. 4M-N and Fig. S7A-B). Additionally, IF staining revealed that ColXIII is expressed in osteocytes of *Col13a1^{oe}* mice but not in WT (Fig. S7C-D) indicating that ColXIII expression in osteocytes disturbs proper differentiation of osteoblasts to osteocytes.

ColXIII overexpression alters osteoblast differentiation and proliferation

The μCT, XPS, and SHG data revealed that overexpression of ColXIII affected bone quantity and quality. Notably, parathyroid hormone levels have been found normal in *Col13a1^{oe}* mice [19],

indicating that hyperparathyroidism is not the cause of the bone defects in the *Col13a1*^{oe} mice. Consequently, altered osteoblast differentiation was considered as a possible cause of the altered bone composition. This hypothesis was tested by culturing primary osteoblasts from *Col13a1*^{oe} and WT femurs in osteogenic medium for 21 days and analyzing their proliferation and differentiation capacity. As expected, the primary osteoblasts extracted from the *Col13a1*^{oe} femurs had higher ColXIII expression than WT cells (Fig. 5A). Also, the soluble ColXIII ectodomain was secreted in the cell culture media (Fig. S8A), as found in other types of cultured cells synthesizing this collagen [11,12]. Additionally, western blot (WB) analysis and immunoelectron microscopy (IEM) demonstrated a higher ColI accumulation in the *Col13a1*^{oe} osteoblast cultures (Fig. 5A and B).

The activity of the primary osteoblasts was studied using an enzyme immunoassay for the determination of N-terminal propeptide of type I procollagen (PINP). The PINP concentrations were significantly higher in the culture media of the *Col13a1*^{oe} osteoblasts confirming increased ColI synthesis (Fig. S8B). Furthermore, the *Col13a1*^{oe} osteoblasts had a reduced calcium deposition capacity compared to controls (Fig. 5C) while alkaline phosphatase (ALP, an osteoblast differentiation marker) activity was not changed (Fig. 5D). The diminished mineralization capability and higher ColI production of the primary *Col13a1*^{oe} osteoblasts suggest that disturbed osteoblast differentiation results in altered bone composition in the *Col13a1*^{oe} mice.

Primary *Col13a1*^{oe} osteoblasts had a 1.5-fold higher proliferation rate compared to WT osteoblasts (Fig. 5E and Fig. S9). To examine this finding further, we treated osteoblasts with various signaling pathway inhibitors (Fig. 5E). We found that JNK inhibition by SP600125 (5 μM) and inhibition of MEK1/2, an upstream kinase of ERK1/2, by PD184352 (5 μM) reduced the proliferation rate of primary *Col13a1*^{oe} osteoblasts to the basal level. Wortmannin (1 μM), an inhibitor of PI3Ks, did not

have a significant effect on ColXIII-induced proliferation. Moreover, a β1-integrin blocking antibody (HM β1-1, 2.5 μg/ml) attenuated the ColXIII induced proliferation of osteoblasts (Fig. 5E). Consistent with the *in vitro* studies, histomorphometry analysis of 4-week-old mice revealed a 2-fold increase in the number of osteoblasts divided per bone perimeter (N.Ob/B.Pm) in the *Col13a1*^{oe} vertebrae compared to WT mice (Fig. 5F). Overall, these findings suggested that ColXIII has a role at early stages of osteoblast differentiation and supported our XPS and μCT results.

ColXIII increases bone angiogenesis through β1-integrin-JNK-VEGF pathways

To study the ColXIII-related signaling pathways further, we treated MC3T3-E1 mouse pre-osteoblastic cells with conditioned media (CM) of CHO cells overexpressing ColXIII (*COL13A1*^{oe}-CHO)[8,31]. ColXIII treatment increased the phosphorylated-JNK to total-JNK ratio (pJNK/JNK) by 2-fold as compared to the control treatment, indicating that soluble ColXIII ectodomain activated the JNK pathway (Fig. 5G). Furthermore, adding *COL13A1*^{oe}-CHO CM to MC3T3-E1 cells increased the phosphorylated-ERK to total-ERK ratio (pERK/ERK) (Fig. 5H), while it had no significant effect on the pAkt/Akt ratio (Fig. 5I). Of note, the *COL13A1*^{oe}-CHO CM supplement significantly increased the VEGF protein expression in the MC3T3-E1 osteoblasts (Fig. 5J), suggesting an association for the increased vascularization of the *Col13a1*^{oe} long bones observed by rhodamine and CD31 staining (Fig. 4I-L, Fig. S6E-F) and for the positive correlation between *COL13A1* expression and *VEGF* expression in hMSCs (Fig. 1D). In line with these results, IHC staining revealed enhanced VEGF expression in the *Col13a1*^{oe} mouse tibia where VEGF localizes similarly in both genotypes: primarily on the endosteal osteoblasts, vessels in the endosteum, and on the blood vessels inside the cortical bone (Fig. 4M-N).

To determine the mechanism of action of how ColXIII regulates angiogenesis, we utilized the fetal mouse metatarsal angiogenesis assay [32]. Results showed that metatarsals isolated from the *Col13a1*^{oe} mice had a 2.4-fold increase in the vessel area at culture day 7 as compared to WT controls (Fig. 6A-C). To study the ColXIII related molecular mechanisms, we treated the metatarsals with JNK inhibitor SP600125 and a β1-integrin function blocking antibody. Inhibiting the JNK pathway or β1-integrins equalized the vascular area between the *Col13a1*^{oe} and control metatarsals (Fig. 6C-G). Additionally, we studied the localization of ColXIII in the metatarsal assay and found it on the cell layer under the metatarsal and on the cells localized on the bone surface, indicating that mainly osteoblasts expressed ColXIII (Fig. 6H-I). The localization of ColXIII was similar in WT and in *Col13a1*^{oe} metatarsal cultures but the staining was much more prominent in the *Col13a1*^{oe} cultures.

Col13a1^{oe} osteoblasts boost osteoclast resorption activity

As the μCT images showed severe endocortical bone loss in *Col13a1*^{oe} mice (Fig. 2A), we investigated osteoclast activity by studying the effect of CM from *Col13a1*^{oe} or WT osteoblast on primary WT osteoclasts *in vitro.* We analyzed the number of multinuclear tartrate-resistant acid phosphatase (TRAP) positive cells, considered as osteoclasts (Fig. 7A-B), and resorption pits on bovine bone chips (Fig. 7C-D). Notably, exposure of osteoclasts to the CM from *Col13a1*^{oe} osteoblasts or *COL13A1*^{oe}-CHO cells did not significantly alter the number of multinuclear TRAP positive cells as compared to controls (Fig. 7A, B and E). However, the resorbed area was significantly increased in response to the CM of *Col13a1*^{oe} osteoblasts (Fig. 7C, D and F), while the CM of *COL13A1*^{oe}-CHO had no effect on the resorption when compared to the respective controls. These experiments suggest that the ColXIII ectodomain did not directly affect osteoclastogenesis or resorption activity but that it did alter the

spectrum of molecules secreted by *Col13a1*^{oe} osteoblasts, thus impacting on the osteoclastic-niche and resorption activity.

Discussion

The identification of increased ColXIII expression in osteoporotic patients and, on the other hand, a bone overgrowth turning to drastic bone loss in mice overexpressing ColXIII identifies this collagen as a novel important factor in both regulation of bone growth and pathogenic mechanisms of bone loss (Fig. 8).

In humans, we found that *COL13A1* expression was increased in osteoporotic patients compared to age matched control donors, and this increase correlated positively with osteoporosis-related genes such as *COL1A1* [21], *RUNX2* [2,33,34], and *VEGF* [35]. The latter correlation is particularly suggestive, as in our mouse model we observed that an age-dependent osteoporotic-like phenotype, such as progressive endocortical bone loss, major decrease in cortical thickness, and decreasing total bone volume, was paralleled by the increased expression of VEGF in response to ColXIII. Among its many effects, VEGF exerts several bone-specific activities [36,37] which could explain the majority (if not the totality) of the effects observed in *Col13a1*^{oe} mice. We propose that *Col13a1*^{oe} osteoblasts trigger VEGF upregulation as a consequence of an autocrine/paracrine loop governed by ColXIII itself: when its ectodomain bind to β1 subunit-containing integrin dimers, a signal is transduced via the JNK and ERK pathways and VEGF is produced. In turn, VEGF enhances bone angiogenesis [35] and activates osteoclast resorption activity [36,38-40].

Osteoclasts are responsible for bone resorption and their increased activity could cause the severe bone loss found in the aged *Col13a1*^{oe} mice [41]. The present finding on bone loss and the previous observation that the *Col13a1*^{oe} osteoclasts action is normal *in vitro* [19] collectively suggest that the microenvironment of *Col13a1*^{oe} mice could stimulate osteoclasts. Accordingly, we report here that *Col13a1*^{oe} osteoblasts–derived conditioned medium activated bone resorption by WT osteoclasts *in*

vitro, though we also found that the ColXIII ectodomain had no direct effect on these cells. The role of VEGF is supported by the fact that the main osteoclast stimulating agents, M-CSF and RANKL, enhance both osteoclastogenesis and resorption activity in particular assay [42-44], whereas VEGF increases resorption activity only [36]. In addition to ColXIII and VEGF, hormones such as Irisin [45] and parathyroid hormone [46] are comparable examples of molecules that both stimulate resorption and act as bone anabolic agents. For an example, irisin is suggested to be treatment for osteoporosis as an anabolic agent or as a drug target: blocking irisin might prevent bone resorption and subsequently, bone loss [45]. Our findings indicate that blocking the enhanced ColXIII activity in osteoblasts could prevent excessive bone resorption and bone loss. To study this hypothesis further, our subsequent aim is to investigate how the absence of soluble ColXIII affects skeletal development and bone remodeling using loss-of-function mouse models.

Notably, in *Col13a1*^{oe} mice and in the metatarsal angiogenesis assay, we observed a significant neoangiogenic drive which was the result of activation of JNK pathway and increased VEGF production. Bone formation is strongly coupled with bone angiogenesis, especially in long bones [47-50] and the main growth factor regulating angiogenesis in bone tissue is osteoblast-derived VEGF [1,35,51,52]. Overexpression of VEGF in osteoprogenitors causes high bone mass phenotype in mice [53], and the excessive bone formation observed in *Col13a1*^{oe} mice partly resembles these previously described phenotypes of VEGF overexpression mouse lines. Conditional overexpression of VEGF under control of *Col1a1* [54], *Col2a1* or *Runx2* [53] promoters in mouse fetuses results in abnormally short and thick long bones, disturbed formation of cortical bone with trabecular-like structures (similar as in *Col13a1*^{oe} mice), high density of CD31^{+} vasculature and death at birth. Likewise, VEGF overexpression under *Col2a1*-cre induced after birth results in a replacement of metaphyseal cortical bone with porous trabecular material [53]. The VEGF overexpression causes an increased thickening of

diaphyseal area of the long bones [53,54], the same anatomical zone where the bone growth of the *Col13a1*^{oe} mice is the most prominent. Moreover, VEGF overexpression mice had enhanced bone resorption activity at the diaphyseal cortical bone and reduced resorption in the metaphysis. Furthermore, mice lacking the von Hippel–Lindau (VHL) gene (a regulator of hypoxia inducible factor-1 stabilization)[55] in osteoblasts have a high bone mass phenotype with vastly vascularized long bones caused by high expression of VEGF [56]. Additionally, activation of the HIF pathway in osteoblasts and subsequent elevated VEGF levels disturb the integrity of the osteocyte network [57]. Hence, based on the observations *in vitro* and *in vivo*, it seems plausible that VEGF produced by *Col13a1*^{oe} osteoblasts is the key soluble factor responsible for increased bone angiogenesis and osteoclast activity that we observed here. It is also worth mentioning that we have not observed an abnormal vascular phenotype in the *Col13a1*^{oe} mice in other tissues, such as skin (either healthy or during wound healing), heart, or retina, even though the ColXIII transgene expression is also high in those tissues (Auvinen A-M. *et al*., unpublished). Thus, it seems that the tubular bones are especially sensitive to ColXIII-triggered proangiogenic effects.

Our data reveals that the ColXIII ectodomain regulates osteoblasts, osteocytes and, indirectly, osteoclast resorption activity. Basic multicellular units (BMUs) are transient anatomic groups of osteoblasts and osteoclasts [58] that manage endosteal bone turnover in young and old mice [59]. Advancing age affects the BMU bone formation balance, resulting in cortical porosity and reduced cortical thickness [59,60]. Additionally, aging is associated with reduced osteocyte number and connectivity in mouse cortical bone [61], and osteocytes are known to directly affect BMUs via RANKL, sclerostin, osteocyte autophagy, and osteocyte apoptosis [4,62]. Ablation of osteocytes in animal models results in intracortical porosity, microfractures, osteoblastic dysfunction, and trabecular bone loss [63]. Thus, the drastic endocortical bone loss seen in the *Col13a1*^{oe} mouse femurs,

resembling osteoporosis in humans [6,64], could be attributed to either altered BMU function or deterioration of the osteocyte network, or more likely to both as they are entwined. Our data indicates that overexpression of ColXIII in osteoblasts and osteocytes disturbs proper differentiation of the osteoblast-osteocyte lineage and leads to deterioration of the lacuna-canalicular network. Interestingly, cortical bone loss in the *Col13a1*^{oe} mice was not accompanied by bone loss in the trabecular bone compartment. In fact, it is known that both the structure of BMUs and bone remodeling processes are different and unique in cortical and trabecular bone [58], and that gender and genetic background affect age-related bone loss in cortical bone but not in trabecular bone [59]. Consequently, it appears that ColXIII affects mostly BMU-based cortical bone remodeling. In line with these observations, we further showed that there was slightly less trabecular bone in the 4-week-old mouse femurs of both *Col13a1*^{oe} genders, but this quantity grew over time and significantly overcame WT littermates in elderly *Col13a1*^{oe} mice. These data indicate that overexpression of ColXIII to some extent promotes the preservation of trabecular bone during aging, especially in females.

Overall, our findings indicate that ColXIII appears to affect osteoblasts, osteocytes, and osteoclasts with diverse effects on bone quantity and quality over time. Data presented here suggest that ColXIII regulated the development of the bone vasculature and affected osteoblast-osteoclast crosstalk. High expression of ColXIII clearly increased bone formation in young animals, but subsequently disturbed the proper bone maturation and homeostasis and led to an osteoporotic phenotype in senescent *Col13a1*^{oe} mice. To summarize, in this study, we show that ColXIII is a regulator of cortical bone remodeling and angiogenesis, with possible implications in osteoporosis.

Materials and methods

Bioinformatics

Unprocessed microarray data of hMSCs from healthy middle-aged (42–67 years old), healthy elderly (79–89 years old), elderly osteoporotic donors (79–94 years old) (n = 5 for middle-aged, osteoporotic and *in vitro* senescent hMSC; n = 4 for elderly) were downloaded from GEO (accession GSE35959)[21], imported into Chipster software and normalized using the robust multi-array average algorithm. The putative *COL13A1* probe "211343_s_at" was removed prior to further analyses as it overlapped completely with a sequence from *COL4A1*, and the remaining probes for each gene analyzed were averaged into a single value by the geometric mean. Per each gene, the normality of distribution was evaluated using the D'Agostino-Pearson omnibus test. Pearson correlation (for normally-distributed data) or Spearman's rank correlation (for non-normally-distributed data) analysis and ANOVA followed by false discovery rate (FDR) were used to further investigate the data.

Mouse lines and maintenance

Generation of the transgenic *Col13a1*^{oe} has been previously published [19]. C57BL/6J-back crossed (>10 generations) mice of both sexes were used in the experiments and WT littermates were used as controls. For this, transgene-positive *Col13a1*^{oe} males were bred with C57BL/6J females. Mice were housed in the University of Oulu specific pathogen-free animal facility. The mouse line is publicly available in the Infrafrontier EMMA repository with the strain name B6.Cg-Tg(Col13a1)2Pih/Oulu (EM:09885).

Bone morphology

Left femurs of *Col13a1*^{oe} and WT littermates were imaged with a Skyscan 1176 scanner (Bruker microCT, Belgium) for morphological assessment by following the guidelines for assessment of bone

microstructure in rodents [65]. Number of mice analyzed ordered by increasing age: male WT (6, 4, 6, 4, 6), male *Col13a1*^{oe} (5, 4, 7, 7, 5), female WT (4, 4, 5, 5, 4), female *Col13a1*^{oe} (6, 4, 6, 7, 6). The X-ray tube voltage was set to 50kV and a 0.5mm aluminum filter was applied. Projection images were collected every 0.3 degrees over a 360-degree rotation with an exposure time of 4000 ms. All image processing was performed with the manufacturer's software package. Femur length was measured (Dataviewer v. 1.5.6.2, Bruker, Belgium) from the top of trochanter major in the mid-frontal plane to the distal patellofemoral groove. The measurement was repeated three times, and the mean was used as the final result. Morphometric analyses were done using CTAn software (Skyscan v. 1.11.10.0, Bruker, Belgium). Trabecular bone was manually segmented by drawing regions of interest extending 0.9mm toward diaphysis from distal femoral growth plate.

Due to longitudinal growth, two different lengths of volumes of interest (VOIs) were used for cortical bone analysis. The trochanter major was used as an anatomical landmark, and VOI selection continued distally 3.6 mm for the 4-week time point and 5.4 mm for other time points. The bone tissue was thresholded and despeckled and VOIs for cortical bone were refined with structural parameters. A 3D structural analysis was performed to define trabecular bone BV/TV and Tb.N, while Ct.Ar, Ma.Ar, and Ct.Th were measured with 2D structural analysis.

XPS

Mouse femurs were dissected, soft tissue was removed, and 1mm thick cortical bone slices from mid-diaphysis were cut by using a slow speed diamond saw. Bone slices were cleaned in PBS with an ultrasonic bath. Following sonication, the bone chips were washed with MilliQ water, dehydrated in ethanol series, and dried in a vacuum. XPS spectra were collected with the ESCALAB 250Xi XPS System (Thermo Fisher Scientific, USA) by using the monochromatic Al Kα (1486.6 eV) X-ray source and a 200 µm spot size from matching anterior sites of bone samples. The spectrometer was operated in

constant analyzer energy (CAE) mode. Wide energy range survey spectra and high-resolution elemental spectra were recorded with 150 eV and 20 eV pass energies, respectively. The base pressure of the vacuum chamber was 3x10-9 mbar. The relative atomic percentage concentrations of carbon (C1s), calcium (Ca2p), nitrogen (N1s), oxygen (O1s) and phosphorus (P2p) were calculated from the XPS data by using Avantage (Thermo Fisher Scientific, USA) XPS data analysis software.

Cell culture

Mouse primary osteoblast cultures were prepared from the femurs of 4-week-old WT and *Col13a1*^{oe} mice as previously described [66]. Briefly, femurs were dissected out, and soft tissue and periosteum were carefully removed. The cartilage ends of the bones were cut off, and the bone marrow was removed by aspirating with PBS. Cleaned bones were cut into small pieces and briefly digested with collagenase (2 mg/ml in α-MEM) for 2 h at 37 °C. The bone chips were washed with PBS and cultured in 6-well plates in α-MEM (Gibco, USA) supplemented with 10% FBS (Gibco, USA) and 1X of penicillin and streptomycin (Sigma, USA). The bone chips were not disturbed for 3 days to allow migration of osteoblast onto the culture dish. From then on, medium was changed every 2-3 days. The bone chips were on the dish until the first passage at day 7. Subsequently, cells grown out of the chips were subcultured before reaching confluence. Experiments were performed using cells from passages 2–3.

For osteogenic differentiation studies, primary bone cells were cultured up to 21 days in osteogenic medium (α-MEM supplemented with 10% FBS, 1X penicillin and streptomycin, ascorbic acid 50 μg/ml and 10 mM of β-glycerophosphate) on 24-well plates. The seeding density was 40 000 cells/well.

CHO-cells (ATCC, USA) stably expressing enhanced green fluorescent protein (EGFP) or ColXIII tagged with EGFP (*COL13A1*^{oe}-CHO) have been described previously[8,31]. CHO-cells were cultured in α-MEM supplemented with 10% FBS, 1X penicillin and streptomycin, and 50 μg/ml of ascorbic acid. Serum-free conditioned media was prepared as previously described [8,31].

For immunofluorescence staining primary osteoblasts were grown on glass coverslips. They were fixed with 3% PFA and stained for vinculin (#V9131 Sigma, USA) or actin using a phallotoxin probe, Alexa Fluor 488 phalloidin (#A12379, Molecular Probes, USA) with methods provided by the manufacturer.

MC3T3-E1 murine osteoblastic cell line (ATCC) was cultured in α-MEM (Gibco, USA) supplemented with 10% FBS (Gibco, USA) and 1X of penicillin and streptomycin (Sigma, USA). For signaling pathway studies, 200 000 cells per well of MC3T3-E1 cells were seeded on 6-well plates and on the following day, treated with 30% of *COL13A1*^{oe}-CHO or control CM for 1 h or 24 h. MC3T3-E1 and CHO cells were regularly tested for mycoplasma contamination.

Western blotting

Cells were washed with cold PBS and subsequently extracted in RIPA lysis buffer (Cell Signaling Technology, USA) supplemented with Phenylmethylsulfonyl fluoride (Sigma, USA) and Phosphatase Inhibitor Cocktail Set V (Calbiochem, USA). Protein lysates were analyzed by SDS-PAGE followed by WB with antibodies specific to ColXIII[7], pERK (#4370), ERK (#4695), pAkt (#4060), Akt (#4691), pJNK (#4668), JNK (#9252) (Cell Signaling Technology, USA), VEGF (#ab46154, Abcam, UK), β-tubulin (MA5-16308, Invitrogen, USA), ColI (#sc-8787), HA-tag (#sc-805), PCNA (#sc-56), and β-actin (#sc-1616, Santa Cruz Biotechnology, USA).

Immunoelectron microscopy

IEM samples were prepared with the Tokuyasu cryosectioning technique [67]. Primary osteoblasts were fixed in 4% paraformaldehyde in 0.1 M phosphate buffer (pH 7.4) with 2.5% sucrose. Fixed cells were rinsed with PBS and mixed with 12% gelatine in PBS. After 10 min incubation at room temperature, cells were pelleted by centrifugation, and the gelatin was solidified on ice for 30 min. Pellets were cut into small pieces and immersed in 2.3 M sucrose in PBS and rotated at 4 °C for 4 h. Thin cryosections were labeled with ColI antibody (#600-401-103-0.1, Rockland, USA) and conjugated gold markers to visualize antibody-binding with the Tecnai Spirit transmission electron microscope (FEI Company, USA) with a Quemesa CCD camera (Olympus, Japan).

Mouse PINP enzyme immunoassay

Primary osteoblasts were cultured in osteogenic medium and PINP concentrations were measured from culture media after 7, 14 and 21 days in subculture. Culture media samples were centrifuged briefly and stored at –20 °C. Undiluted samples were analyzed using Rat/Mouse PINP EIA kit (IDS, UK) according to the manufacturer's instructions.

Alkaline phosphatase activity

ALP activity was measured from cell lysates as described earlier [68]. Briefly, cells grown in osteogenic media on 24-well plates were lysed by assay buffer (0.1% Triton X-100, PH 7.6) and rapidly frozen. Thawed cell lysates were analyzed for ALP activity using 0.1 mM 4-*p*-nitrophenylphosphate (Sigma, USA) as the substrate and quantified at 405 nm in a 1420 Victor^{TM} multilabel plate reader (PerkinElmer Life Sciences/Wallac, USA). The protein concentration of the samples was determined using the Pierce BCA Protein Assay kit (Thermo Scientific, USA). ALP activity is expressed as units/mg protein.

Calcium measurement

Primary osteoblasts grown in osteogenic media on 24-well plates were washed three times in PBS and incubated in 0.6 M HCl overnight. Attained cell extracts were complexed with o-cresolphthalein-complexon (Roche Diagnostics, Switzerland) according to the manufacturer's instructions. The colorimetric reaction was quantified at 570 nm in a 1420 Victor^{TM} multilabel plate reader (PerkinElmer Life Sciences/Wallac, USA).

Cell proliferation

Primary osteoblasts (5000 cells per well) were plated on 96-well plates, treated with SP600125, PD184352 (5 μM, Sigma, USA), Wortmannin (1 μM, Sigma, USA) or β1 blocking antibody (HM β1-1, 2.5 μg/ml, #562219, BD Pharmingen, USA), and cultured in normal growth media. Proliferation was followed with IncuCyte live cell imaging system (Essen Bioscience, USA) for 72 h as described previously [69,70]. Analysis was performed using IncuCyte Zoom 2015A software (Essen Bioscience, USA). Results are shown as a percent of cell confluence. The size of the cells is comparable between the genotypes (Fig. S9).

Tissue staining and histomorphometry

Bone histomorphometry analyses were performed on L4 vertebrae as described previously [71]. Briefly, lumbar vertebrae of 4-week-old mice were dissected, and soft tissue was removed. Vertebrae were fixed for 24 h in 4% paraformaldehyde at 4 °C, dehydrated in ethanol series, and embedded in PMMA resin according to standard protocols [72]. Osteoblast and trabecular bone parameters were analyzed on sections stained by toluidine blue. Analyses were performed using the Osteomeasure Analysis System (Osteometrics, USA) according to standard protocols described previously [71].

For rhodamine staining, femurs were dissected, and soft tissue was removed. Next, the samples were fixed for 24 h in 4% paraformaldehyde at 4 °C. Rhodamine 6G (Sigma, USA) was dissolved (0.002 %) in MMA and used as a staining solution in the first pre-infiltration. After the 6-day infiltration and three solution changes, bone samples were embedded in PMMA. Subsequently, PMMA-blocks were imaged using a confocal microscope (FluoView FV1000, Olympus, Japan and LSM 780, Zeiss, Germany). Maximum intensity projections were created with the ImageJ software (NIH, USA). Rhodamine spreads throughout the lacunar-canalicular network and blood vessels, and subsequently, binds to cell membranes and mineral edges revealing the cellular structures in bone.

For SHG imaging, mouse tibias were dissected, soft tissue was removed and samples were fixed 24 h in 4% paraformaldehyde at 4 °C. SHG of the cortical bone was recorded from the anatomically comparable anterior sites of the mid-diaphysis with a multiphoton microscope (A1R MP+; Nikon, Japan).

IF of CD31 in cryo-sections was done from femurs of 12-week-old mice according to previously published protocol [73]. Briefly, femurs were dissected from mice, soft tissue was removed and samples were fixed with 4% ice-cold paraformaldehyde solution for 4 h on ice. Next, the samples were washed with PBS and subsequently decalcified in EDTA. Then, samples were washed with PBS to remove EDTA and incubated in cryoprotectant solution (200 g of sucrose and 20 g of polyvinylpyrrolidone in 1000 ml of PBS) for 24 h at 4 °C. Next, samples were embedded in solution containing 8 g of gelatin, 2 g of polyvinylpyrrolidone and 20 g of sucrose in 100 ml of PBS, incubated 30 min in room temperature and then frozen. 70 μm sections were cut using cryotome CM3050S

(Leica, Germany), stained for CD31 (#550274, BD Pharmingen, USA) and subsequently imaged using a confocal microscope (LSM 780, Zeiss, Germany).

IHC of VEGF in paraffin-sections was done from tibia of 4-week-old mice. Samples were fixed 24 h in 4% paraformaldehyde at 4 °C, washed with water, and decalcified in EDTA. Decalcified samples were dehydrated, paraffin embedded, and sectioned. Then, 5 μm sections were deparaffinizated, rehydrated in ethanol and subsequently stained with VEGF (#1316, Abcam, UK) using HistoMouse-kit (Thermo Scientific, USA) according to the manufacturer's protocol or with hematoxylin and eosin. Sections were imaged using an upright light microscope DM LB2 (Leica Microsystems, Germany) or Axio Imager (Zeiss, Germany).

Scanning electron microscopy

Acid etching protocol and visualization of the lacunar-canalicular network has been described previously [74]. PMMA-embedded mouse vertebrae were acid-etched in 9% phosphoric acid for 30 seconds followed by careful 5-minute immersion in sodium hypochlorite and two brief washings with water. Specimens were dried using a critical point dryer and samples were coated with 5 nm platinum by with the Q150T ES sputter coater (Quorum Technologies, UK) and observed with the Sigma HD VP FE-SEM (Zeiss, Germany).

Metatarsal assay

The mouse metatarsal angiogenesis assay was performed as previously described [32]. Metatarsals were isolated from E17.5 fetuses and plated on Col1 (Sigma, USA) coated tissue culture plates (Corning, USA) and covered with α-MEM (Gibco, USA) supplemented with 10% of FBS and 1X penicillin and streptomycin (Sigma, USA). On the following day, the medium was changed and the

metatarsals were treated with respective inhibitors (SP600125 and PD184352, 5 μM, Sigma, USA), vehicle, or β1 blocking antibody (HM β1-1, 2.5 μg/ml, #562219, BD Pharmingen, USA). The medium was changed every second day until day 7. Then, metatarsal cultures were fixed with 4% paraformaldehyde and stained for CD31 (#550274, BD Pharmingen, USA) and nuclei (DAPI, Sigma, USA), as previously described [32]. Metatarsals were imaged using a confocal microscope (LSM 780, Zeiss, Germany). Maximum intensity projections from metatarsal Z-stacks were done with the ImageJ software (NIH, USA) and median filter (radius 3) was used to remove background noise. Subsequently, the images were made binary, the CD31 stained vessel area was analyzed with the ImageJ and vessel area was normalized to bone size as previously described [32]. For ColXIII, metatarsal cultures were stained using antibodies specific to ColXIII [7] and the Alexa Fluor 488 Tyramide SuperBoost-kit (Invitrogen, USA) according to the manufacturer's protocol.

Osteoclast resorption assay

The osteoclast resorption assays have been described earlier [75,76]. Briefly, the bone marrow of six 8- to 10-week-old BL/6J female mice was isolated from tibias and femurs. Next, bone marrow cell suspension was incubated on a cell culture plate in 37 °C for 3 hours, and subsequently, nonadherent, hematopoietic cells were collected for osteoclast differentiation assay. Hematopoietic cells were seeded on 96-well plates, containing round bovine bone slices (Lehenkari Consulting, Finland). Cells were cultured in α-MEM (Gibco, USA) supplemented with 10% of FBS and 1X penicillin and streptomycin (Sigma, USA). Osteoclast differentiation was induced with 30 ng/ml RANKL (Peprotech, USA) and 10 ng/ml M-CSF (R&D Systems, USA). Cells were treated with CM form *COL13A1*^{oe}-CHO, CHO, *Col13a1*^{oe} osteoblasts, or WT osteoblasts. Cells were cultured for 7 days, washed with PBS and fixed with 4% PFA. Bone chips were stained for TRAP using an acid phosphatase leukocyte kit (Sigma) and imaged with a microscope (Axio Imager; Zeiss, Germany). The number of multinuclear (three or more

nuclei) TRAP positive cells, considered as osteoclasts [36,77], was counted using ImageJ. After light microscopic imaging, cells were detached by brushing, and bone chips were dehydrated in ascending ethanol series and air-dried. Bone samples were coated with 5 nm platinum by Q150T ES sputter coater (Quorum Technologies, UK) and observed with Sigma HD VP FE-SEM (Zeiss, Germany). SEM images were taken from three fields (voltage 5.0 kV, magnification 50x) of each bone slice. Resorption pit areas were determined from SEM images with a Merz grid analysis using ImageJ as previously described [76]. A Merz grid with 96 grid-points in semicircular lines was put over the image. Points in pits were counted and the percentage of resorption pits against intact bone surface was calculated. The quantity of resorbed area was normalized to a multinuclear TRAP positive cell number.

Statistics

Graphical data are shown as box-plots representing the 25th –75th percentile values. The line in the box denotes the median value. Whiskers represent the complete spread of all samples in the group (min to max). Statistical significance was determined by the Student's t-test and one-way or two-way ANOVA followed by the Benjamini, Krieger and Yekutieli FDR post hoc test [78]. Values of $p < 0.05$ or FDR-corrected $p\ (q) < 0.05$ values were considered statistically significant; n denotes the number of animals, the number of parental animals in primary cell and tissue cultures, or the number of repeated experiments. No statistical methods were used to predetermine sample size. The experiments were not randomized and the investigators were not blinded.

Study approval

Permission (ESAVI/4220/04.10.07/2013) for the maintenance of mice was obtained from the Finnish Animal Care and Use Committee. All the mouse experiments complied with the European Community

Council Directive (September 22, 2010; 2010/63/EEC), national legislation and the regulations for the care and use of laboratory animals.

Acknowledgements

We greatly acknowledge professor G. Karsenty for helpful advice and support throughout the project and for critical reading of this manuscript. We also thank professor J. Tuukkanen for helpful discussions. V.-P. Ronkainen and A. Viklund are acknowledged for their assistance with confocal imaging and image analysis, M. Seppänen, S. Vilmi, and A. White for their technical assistance. We thank M. Bassignana for the graphical abstract. This work was supported by grants from Biocenter Oulu, the Sigrid Jusélius Foundation, and the Academy of Finland (grants no. 294617 and 284605). We also acknowledge the Biocenter Oulu Light and Electron Microscopy Core Facilities, Biocenter Finland, the University of Oulu Animal Facility, and the Center of Microscopy and Nanotechnology at the University of Oulu for expert help and access to equipment.

Author contributions

Conceptualization J.K. and A.V.K.; Investigation J.K., A.V.K., V.I., M.F., R.K-F., H.P., H.H., A.H., H.T., R.S., I.M. and E.K.; Formal Analysis and Visualization J.K., A.V.K., M.F. and V.I.; Writing – Original Draft J.K., A.V.K. and R.K-F.; Writing – Review & Editing J.K., A.V.K., V.I., M.F., A.H., I.M., E.K., S.S. and T.P.; Funding Acquisition J.K., S.S. and T.P.; Supervision T.P.

Competing interests

The authors declare no competing interests.

[1] Karsenty, G., Wagner, E.F., 2002. Reaching a genetic and molecular understanding of skeletal development. Dev. Cell. 2 389-406.

[2] Karsenty, G., Kronenberg, H.M., Settembre, C., 2009. Genetic control of bone formation. Annu. Rev. Cell Dev. Biol. 25 629-648.

[3] Long, F., 2011. Building strong bones: molecular regulation of the osteoblast lineage. Nat. Rev. Mol. Cell Biol. 13 27-38.

[4] Bonewald, L.F., 2011. The amazing osteocyte. J. Bone Miner. Res. 26 229-238.

[5] Seeman, E., 2003. Invited Review: Pathogenesis of osteoporosis. J. Appl. Physiol. (1985) 95 2142-2151.

[6] Zebaze, R.M., Ghasem-Zadeh, A., Bohte, A., Iuliano-Burns, S., Mirams, M., Price, R.I., Mackie, E.J., Seeman, E., 2010. Intracortical remodelling and porosity in the distal radius and post-mortem femurs of women: a cross-sectional study. Lancet 375 1729-1736.

[7] Hägg, P., Rehn, M., Huhtala, P., Väisänen, T., Tamminen, M., Pihlajaniemi, T., 1998. Type XIII collagen is identified as a plasma membrane protein. J. Biol. Chem. 273 15590-15597.

[8] Tu, H., Huhtala, P., Lee, H.M., Adams, J.C., Pihlajaniemi, T., 2015. Membrane-associated collagens with interrupted triple-helices (MACITs): evolution from a bilaterian common ancestor and functional conservation in C. elegans. BMC Evol. Biol. 15 3.

[9] Nykvist, P., Tu, H., Ivaska, J., Kapyla, J., Pihlajaniemi, T., Heino, J., 2000. Distinct recognition of collagen subtypes by alpha(1)beta(1) and alpha(2)beta(1) integrins. Alpha(1)beta(1) mediates cell adhesion to type XIII collagen. J. Biol. Chem. 275 8255-8261.

[10] Tu, H., Sasaki, T., Snellman, A., Gohring, W., Pirila, P., Timpl, R., Pihlajaniemi, T., 2002. The type XIII collagen ectodomain is a 150-nm rod and capable of binding to fibronectin, nidogen-2, perlecan, and heparin. J. Biol. Chem. 277 23092-23099.

[11] Snellman, A., Tu, H., Väisänen, T., Kvist, A.P., Huhtala, P., Pihlajaniemi, T., 2000. A short sequence in the N-terminal region is required for the trimerization of type XIII collagen and is conserved in other collagenous transmembrane proteins. EMBO J. 19 5051-5059.

[12] Väisänen, M.R., Väisänen, T., Pihlajaniemi, T., 2004. The shed ectodomain of type XIII collagen affects cell behaviour in a matrix-dependent manner. Biochem. J. 380 685-693.

[13] Härönen, H., Zainul, Z., Tu, H., Naumenko, N., Sormunen, R., Miinalainen, I., Shakirzyanova, A., Oikarainen, T., Abdullin, A., Martin, P., Santoleri, S., Koistinaho, J., Silman, I., Giniatullin, R., Fox, M.A., Heikkinen, A., Pihlajaniemi, T., 2017. Collagen XIII secures pre- and postsynaptic integrity of the neuromuscular synapse. Hum. Mol. Genet. 26 2076-2090.

[14] Väisänen, T., Väisänen, M.R., Pihlajaniemi, T., 2006. Modulation of the cellular cholesterol level affects shedding of the type XIII collagen ectodomain. J. Biol. Chem. 281 33352-33362.

[15] Väisänen, M.R., Väisänen, T., Tu, H., Pirila, P., Sormunen, R., Pihlajaniemi, T., 2006. The shed ectodomain of type XIII collagen associates with the fibrillar fibronectin matrix and may interfere with its assembly in vitro. Biochem. J. 393 43-50.

[16] Hägg, P., Väisänen, T., Tuomisto, A., Rehn, M., Tu, H., Huhtala, P., Eskelinen, S., Pihlajaniemi, T., 2001. Type XIII collagen: a novel cell adhesion component present in a range of cell-matrix adhesions and in the intercalated discs between cardiac muscle cells. Matrix Biol. 19 727-742.

[17] Sund, M., Väisänen, T., Kaukinen, S., Ilves, M., Tu, H., Autio-Harmainen, H., Rauvala, H., Pihlajaniemi, T., 2001. Distinct expression of type XIII collagen in neuronal structures and other tissues during mouse development. Matrix Biol. 20 215-231.

[18] Kalajzic, I., Staal, A., Yang, W.P., Wu, Y., Johnson, S.E., Feyen, J.H., Krueger, W., Maye, P., Yu, F., Zhao, Y., Kuo, L., Gupta, R.R., Achenie, L.E., Wang, H.W., Shin, D.G., Rowe, D.W., 2005. Expression profile of osteoblast lineage at defined stages of differentiation. J. Biol. Chem. 280 24618-24626.

[19] Ylönen, R., Kyrönlahti, T., Sund, M., Ilves, M., Lehenkari, P., Tuukkanen, J., Pihlajaniemi, T., 2005. Type XIII collagen strongly affects bone formation in transgenic mice. J. Bone Miner. Res. 20 1381-1393.

[20] Latvanlehto, A., Fox, M.A., Sormunen, R., Tu, H., Oikarainen, T., Koski, A., Naumenko, N., Shakirzyanova, A., Kallio, M., Ilves, M., Giniatullin, R., Sanes, J.R., Pihlajaniemi, T., 2010. Muscle-derived collagen XIII regulates maturation of the skeletal neuromuscular junction. J. Neurosci. 30 12230-12241.

[21] Benisch, P., Schilling, T., Klein-Hitpass, L., Frey, S.P., Seefried, L., Raaijmakers, N., Krug, M., Regensburger, M., Zeck, S., Schinke, T., Amling, M., Ebert, R., Jakob, F., 2012. The transcriptional profile of mesenchymal stem cell populations in primary osteoporosis is distinct and shows overexpression of osteogenic inhibitors. PLoS One 7 e45142.

[22] Logan, C.V., Cossins, J., Rodriguez Cruz, P.M., Parry, D.A., Maxwell, S., Martinez-Martinez, P., Riepsaame, J., Abdelhamed, Z.A., Lake, A.V., Moran, M., Robb, S., Chow, G., Sewry, C., Hopkins, P.M., Sheridan, E., Jayawant, S., Palace, J., Johnson, C.A., Beeson, D., 2015. Congenital Myasthenic Syndrome Type 19 Is Caused by Mutations in COL13A1, Encoding the Atypical Non-fibrillar Collagen Type XIII alpha1 Chain. Am. J. Hum. Genet. 97 878-885.

[23] Zhang, H., Fredericks, T., Xiong, G., Qi, Y., Rychahou, P.G., Li, J.D., Pihlajaniemi, T., Xu, W., Xu, R., 2018. Membrane associated collagen XIII promotes cancer metastasis and enhances anoikis resistance. Breast Cancer Res. 20 y.

[24] Sund, M., Ylönen, R., Tuomisto, A., Sormunen, R., Tahkola, J., Kvist, A.P., Kontusaari, S., Autio-Harmainen, H., Pihlajaniemi, T., 2001. Abnormal adherence junctions in the heart and reduced angiogenesis in transgenic mice overexpressing mutant type XIII collagen. EMBO J. 20 5153-5164.

[25] Semenov, M., Tamai, K., He, X., 2005. SOST is a ligand for LRP5/LRP6 and a Wnt signaling inhibitor. J. Biol. Chem. 280 26770-26775.

[26] Henss, A., Rohnke, M., Knaack, S., Kleine-Boymann, M., Leichtweiss, T., Schmitz, P., El Khassawna, T., Gelinsky, M., Heiss, C., Janek, J., 2013. Quantification of calcium content in bone by using ToF-SIMS--a first approach. Biointerphases 8 31. Epub 2013 Nov 14.

[27] Nakada, H., Sakae, T., Tanimoto, Y., Teranishi, M., Kato, T., Watanabe, T., Saeki, H., Kawai, Y., Legeros, R.Z., 2012. Assessment of the Quality of Newly Formed Bone around Titanium Alloy Implants by Using X-Ray Photoelectron Spectroscopy. Int. J. Biomater. 2012 615018.

[28] Chen, X., Nadiarynkh, O., Plotnikov, S., Campagnola, P.J., 2012. Second harmonic generation microscopy for quantitative analysis of collagen fibrillar structure. Nat. Protoc. 7 654-669.

[29] Ambekar, R., Chittenden, M., Jasiuk, I., Toussaint, K.C., 2012. Quantitative second-harmonic generation microscopy for imaging porcine cortical bone: comparison to SEM and its potential to investigate age-related changes. Bone 50 643-650.

[30] Kerschnitzki, M., Wagermaier, W., Roschger, P., Seto, J., Shahar, R., Duda, G.N., Mundlos, S., Fratzl, P., 2011. The organization of the osteocyte network mirrors the extracellular matrix orientation in bone. J. Struct. Biol. 173 303-311.

[31] Tu, H., Pirskanen-Matell, R., Heikkinen, A., Oikarainen, T., Risteli, J., Pihlajaniemi, T., 2018. Autoimmune antibodies to collagen XIII in myasthenia gravis patients. Muscle Nerve 57 506-510.

[32] Song, W., Fhu, C.W., Ang, K.H., Liu, C.H., Johari, N.A., Lio, D., Abraham, S., Hong, W., Moss, S.E., Greenwood, J., Wang, X., 2015. The fetal mouse metatarsal bone explant as a model of angiogenesis. Nat. Protoc. 10 1459-1473.

[33] Ducy, P., Zhang, R., Geoffroy, V., Ridall, A.L., Karsenty, G., 1997. Osf2/Cbfa1: a transcriptional activator of osteoblast differentiation. Cell 89 747-754.

[34] Wei, J., Shimazu, J., Makinistoglu, M.P., Maurizi, A., Kajimura, D., Zong, H., Takarada, T., Lezaki, T., Pessin, J.E., Hinoi, E., Karsenty, G., 2015. Glucose Uptake and Runx2 Synergize to Orchestrate Osteoblast Differentiation and Bone Formation. Cell 161 1576-1591.

[35] Hu, K., Olsen, B.R., 2017. Vascular endothelial growth factor control mechanisms in skeletal growth and repair. Dev. Dyn. 246 227-234.

[36] Sipola, A., Nelo, K., Hautala, T., Ilvesaro, J., Tuukkanen, J., 2006. Endostatin inhibits VEGF-A induced osteoclastic bone resorption in vitro. BMC Musculoskelet. Disord. 7 56.

[37] Hu, K., Olsen, B.R., 2016. The roles of vascular endothelial growth factor in bone repair and regeneration. Bone 91 30-38.

[38] Niida, S., Kaku, M., Amano, H., Yoshida, H., Kataoka, H., Nishikawa, S., Tanne, K., Maeda, N., Nishikawa, S., Kodama, H., 1999. Vascular endothelial growth factor can substitute for macrophage colony-stimulating factor in the support of osteoclastic bone resorption. J. Exp. Med. 190 293-298.

[39] Nakagawa, M., Kaneda, T., Arakawa, T., Morita, S., Sato, T., Yomada, T., Hanada, K., Kumegawa, M., Hakeda, Y., 2000. Vascular endothelial growth factor (VEGF) directly enhances osteoclastic bone resorption and survival of mature osteoclasts. FEBS Lett. 473 161-164.

[40] Helmrich, U., Di Maggio, N., Guven, S., Groppa, E., Melly, L., Largo, R.D., Heberer, M., Martin, I., Scherberich, A., Banfi, A., 2013. Osteogenic graft vascularization and bone resorption by VEGF-expressing human mesenchymal progenitors. Biomaterials 34 5025-5035.

[41] Crockett, J.C., Rogers, M.J., Coxon, F.P., Hocking, L.J., Helfrich, M.H., 2011. Bone remodelling at a glance. J. Cell. Sci. 124 991-998.

[42] Kong, Y.Y., Yoshida, H., Sarosi, I., Tan, H.L., Timms, E., Capparelli, C., Morony, S., Oliveira-dos-Santos, A.J., Van, G., Itie, A., Khoo, W., Wakeham, A., Dunstan, C.R., Lacey, D.L., Mak, T.W., Boyle, W.J., Penninger, J.M., 1999. OPGL is a key regulator of osteoclastogenesis, lymphocyte development and lymph-node organogenesis. Nature 397 315-323.

[43] Fuller, K., Kirstein, B., Chambers, T.J., 2006. Murine osteoclast formation and function: differential regulation by humoral agents. Endocrinology 147 1979-1985.

[44] Xiong, J., Piemontese, M., Thostenson, J.D., Weinstein, R.S., Manolagas, S.C., O'Brien, C.A., 2014. Osteocyte-derived RANKL is a critical mediator of the increased bone resorption caused by dietary calcium deficiency. Bone 66 146-154.

[45] Kim, H., Wrann, C.D., Jedrychowski, M., Vidoni, S., Kitase, Y., Nagano, K., Zhou, C., Chou, J., Parkman, V.A., Novick, S.J., Strutzenberg, T.S., Pascal, B.D., Le, P.T., Brooks, D.J., Roche, A.M., Gerber, K.K., Mattheis, L., Chen, W., Tu, H., Bouxsein, M.L., Griffin, P.R., Baron, R., Rosen, C.J., Bonewald, L.F., Spiegelman, B.M., 2018. Irisin Mediates Effects on Bone and Fat via alphaV Integrin Receptors. Cell 175 1768.e17.

[46] Lane, N.E., Sanchez, S., Modin, G.W., Genant, H.K., Pierini, E., Arnaud, C.D., 1998. Parathyroid hormone treatment can reverse corticosteroid-induced osteoporosis. Results of a randomized controlled clinical trial. J. Clin. Invest. 102 1627-1633.

[47] Ramasamy, S.K., Kusumbe, A.P., Wang, L., Adams, R.H., 2014. Endothelial Notch activity promotes angiogenesis and osteogenesis in bone. Nature 507 376-380.

[48] Kusumbe, A.P., Ramasamy, S.K., Adams, R.H., 2014. Coupling of angiogenesis and osteogenesis by a specific vessel subtype in bone. Nature 507 323-328.

[49] Ramasamy, S.K., Kusumbe, A.P., Schiller, M., Zeuschner, D., Bixel, M.G., Milia, C., Gamrekelashvili, J., Limbourg, A., Medvinsky, A., Santoro, M.M., Limbourg, F.P., Adams, R.H., 2016. Blood flow controls bone vascular function and osteogenesis. Nat. Commun. 7 13601.

[50] Langen, U.H., Pitulescu, M.E., Kim, J.M., Enriquez-Gasca, R., Sivaraj, K.K., Kusumbe, A.P., Singh, A., Di Russo, J., Bixel, M.G., Zhou, B., Sorokin, L., Vaquerizas, J.M., Adams, R.H., 2017. Cell-matrix signals specify bone endothelial cells during developmental osteogenesis. Nat. Cell Biol. 19 189-201.

[51] Hu, K., Olsen, B.R., 2016. Osteoblast-derived VEGF regulates osteoblast differentiation and bone formation during bone repair. J. Clin. Invest. 126 509-526.

[52] Grosso, A., Burger, M.G., Lunger, A., Schaefer, D.J., Banfi, A., Di Maggio, N., 2017. It Takes Two to Tango: Coupling of Angiogenesis and Osteogenesis for Bone Regeneration. Front. Bioeng. Biotechnol. 5 68.

[53] Maes, C., Goossens, S., Bartunkova, S., Drogat, B., Coenegrachts, L., Stockmans, I., Moermans, K., Nyabi, O., Haigh, K., Naessens, M., Haenebalcke, L., Tuckermann, J.P., Tjwa, M., Carmeliet, P., Mandic, V., David, J.P., Behrens, A., Nagy, A., Carmeliet, G., Haigh, J.J., 2010. Increased skeletal VEGF enhances beta-catenin activity and results in excessively ossified bones. EMBO J. 29 424-441.

[54] Ben Shoham, A., Rot, C., Stern, T., Krief, S., Akiva, A., Dadosh, T., Sabany, H., Lu, Y., Kadler, K.E., Zelzer, E., 2016. Deposition of collagen type I onto skeletal endothelium reveals a new role for blood vessels in regulating bone morphology. Development 143 3933-3943.

[55] Kaelin, W.G., 2002. Molecular basis of the VHL hereditary cancer syndrome. Nat. Rev. Cancer. 2 673-682.

[56] Wang, Y., Wan, C., Deng, L., Liu, X., Cao, X., Gilbert, S.R., Bouxsein, M.L., Faugere, M.C., Guldberg, R.E., Gerstenfeld, L.C., Haase, V.H., Johnson, R.S., Schipani, E., Clemens, T.L., 2007. The hypoxia-inducible factor alpha pathway couples angiogenesis to osteogenesis during skeletal development. J. Clin. Invest. 117 1616-1626.

[57] Zuo, G.L., Zhang, L.F., Qi, J., Kang, H., Jia, P., Chen, H., Shen, X., Guo, L., Zhou, H.B., Wang, J.S., Zhou, Q., Qian, N.D., Deng, L.F., 2015. Activation of HIFa pathway in mature osteoblasts disrupts the integrity of the osteocyte/canalicular network. PLoS One 10 e0121266.

[58] Sims, N.A., Martin, T.J., 2014. Coupling the activities of bone formation and resorption: a multitude of signals within the basic multicellular unit. Bonekey Rep. 3 481.

[59] Piemontese, M., Almeida, M., Robling, A.G., Kim, H.N., Xiong, J., Thostenson, J.D., Weinstein, R.S., Manolagas, S.C., O'Brien, C.A., Jilka, R.L., 2017. Old age causes de novo intracortical bone remodeling and porosity in mice. JCI Insight 2 10.1172/jci.insight.93771.

[60] Seeman, E., 2013. Age- and menopause-related bone loss compromise cortical and trabecular microstructure. J. Gerontol. A Biol. Sci. Med. Sci. 68 1218-1225.

[61] Tiede-Lewis, L.M., Xie, Y., Hulbert, M.A., Campos, R., Dallas, M.R., Dusevich, V., Bonewald, L.F., Dallas, S.L., 2017. Degeneration of the osteocyte network in the C57BL/6 mouse model of aging. Aging (Albany NY).

[62] Jilka, R.L., O'Brien, C.A., 2016. The Role of Osteocytes in Age-Related Bone Loss. Curr. Osteoporos Rep. 14 16-25.

[63] Tatsumi, S., Ishii, K., Amizuka, N., Li, M., Kobayashi, T., Kohno, K., Ito, M., Takeshita, S., Ikeda, K., 2007. Targeted ablation of osteocytes induces osteoporosis with defective mechanotransduction. Cell. Metab. 5 464-475.

[64] Power, J., Loveridge, N., Lyon, A., Rushton, N., Parker, M., Reeve, J., 2003. Bone remodeling at the endocortical surface of the human femoral neck: a mechanism for regional cortical thinning in cases of hip fracture. J. Bone Miner. Res. 18 1775-1780.

[65] Bouxsein, M.L., Boyd, S.K., Christiansen, B.A., Guldberg, R.E., Jepsen, K.J., Muller, R., 2010. Guidelines for assessment of bone microstructure in rodents using micro-computed tomography. J. Bone Miner. Res. 25 1468-1486.

[66] Lecanda, F., Warlow, P.M., Sheikh, S., Furlan, F., Steinberg, T.H., Civitelli, R., 2000. Connexin43 deficiency causes delayed ossification, craniofacial abnormalities, and osteoblast dysfunction. J. Cell Biol. 151 931-944.

[67] Slot, J.W., Geuze, H.J., 2007. Cryosectioning and immunolabeling. Nat. Protoc. 2 2480-2491.

[68] Leskelä, H.V., Risteli, J., Niskanen, S., Koivunen, J., Ivaska, K.K., Lehenkari, P., 2003. Osteoblast recruitment from stem cells does not decrease by age at late adulthood. Biochem. Biophys. Res. Commun. 311 1008-1013.

[69] Venkannagari, H., Verheugd, P., Koivunen, J., Haikarainen, T., Obaji, E., Ashok, Y., Narwal, M., Pihlajaniemi, T., Luscher, B., Lehtio, L., 2016. Small-Molecule Chemical Probe Rescues Cells from Mono-ADP-Ribosyltransferase ARTD10/PARP10-Induced Apoptosis and Sensitizes Cancer Cells to DNA Damage. Cell. Chem. Biol. 23 1251-1260.

[70] Matsumoto, Y., La Rose, J., Kent, O.A., Wagner, M.J., Narimatsu, M., Levy, A.D., Omar, M.H., Tong, J., Krieger, J.R., Riggs, E., Storozhuk, Y., Pasquale, J., Ventura, M., Yeganeh, B., Post, M., Moran, M.F., Grynpas, M.D., Wrana, J.L., Superti-Furga, G., Koleske, A.J., Pendergast, A.M., Rottapel, R., 2016. Reciprocal stabilization of ABL and TAZ regulates osteoblastogenesis through transcription factor RUNX2. J. Clin. Invest. 126 4482-4496.

[71] Parfitt, A.M., Drezner, M.K., Glorieux, F.H., Kanis, J.A., Malluche, H., Meunier, P.J., Ott, S.M., Recker, R.R., 1987. Bone histomorphometry: standardization of nomenclature, symbols, and units. Report of the ASBMR Histomorphometry Nomenclature Committee. J. Bone Miner. Res. 2 595-610.

[72] Chappard, D., Palle, S., Alexandre, C., Vico, L., Riffat, G., 1987. Bone embedding in pure methyl methacrylate at low temperature preserves enzyme activities. Acta Histochem. 81 183-190.

[73] Kusumbe, A.P., Ramasamy, S.K., Starsichova, A., Adams, R.H., 2015. Sample preparation for high-resolution 3D confocal imaging of mouse skeletal tissue. Nat. Protoc. 10 1904-1914.

[74] Kubek, D.J., Gattone, V.H., Allen, M.R., 2010. Methodological assessment of acid-etching for visualizing the osteocyte lacunar-canalicular networks using scanning electron microscopy. Microsc. Res. Tech. 73 182-186.

[75] Kylmäoja, E., Kokkonen, H., Kauppinen, K., Hussar, P., Sato, T., Haugan, K., Larsen, B.D., Tuukkanen, J., 2013. Osteoclastogenesis is influenced by modulation of gap junctional communication with antiarrhythmic peptides. Calcif. Tissue Int. 92 270-281.

[76] Kylmäoja, E., Nakamura, M., Kokkonen-Puupera, H., Ronkainen, V.P., Lehenkari, P., Tuukkanen, J., 2018. Gap junctional communication is involved in differentiation of osteoclasts from bone marrow and peripheral blood monocytes. Heliyon 4 e00621.

[77] Coustry, F., Posey, K.L., Maerz, T., Baker, K., Abraham, A.M., Ambrose, C.G., Nobakhti, S., Shefelbine, S.J., Bi, X., Newton, M., Gawronski, K., Remer, L., Veerisetty, A.C., Hossain, M.G., Chiu, F., Hecht, J.T., 2018. Mutant cartilage oligomeric matrix protein (COMP) compromises bone integrity, joint function and the balance between adipogenesis and osteogenesis. Matrix Biol. 67 75-89.

[78] Benjamini, Y., Krieger, A.,M., Yekutieli, D., 2006. Adaptive linear step-up procedures that control the false discovery rate. Biometrika 93 491-507.

Figure legends

Figure 1. ColXIII is linked to osteoporosis. *COL13A1* expression in hMSCs obtained from healthy middle-aged (42–67 years old), healthy elderly (79–89 years old), and elderly osteoporotic donors (79–94 years old) and, *in vitro* senescent hMSCs (A); correlation of *COL13A1* with *COL1A1* (B), *RUNX2* (C), *VEGF* (D), *JAGGED1* (E), and *SOST* (F) expression in hMSCs; n = 5 for middle-aged, osteoporotic, and *in vitro* senescent hMSCs, 4 for elderly donors; **q < 0.01 in one-way ANOVA followed by Benjamini, Krieger and Yekutieli False Discovery Rate (FDR). ● middle-aged, ○ elderly, ■ osteoporotic donor, □ *in vitro* senescent (B-F).

Figure 2. *Col13a1*^{oe} mice possess a massive cortical bone overgrowth followed by drastic bone loss with aging. Representative side views and cross-sectional µCT images of WT and *Col13a1*^{oe} female mice femurs at the age of 4, 12, 25, 35 and 72 weeks. A black line indicates the region of the µCT cross-sectional images in the side views of the femurs, scale bars 1 mm (A); µCT analysis of the cortical area (Ct.Ar) (B), the medullar area (Ma.Ar) (C), and the cortical bone thickness (Ct.Th) (D). Number of mice analyzed ordered by increasing age: male WT (6, 4, 6, 4, 6), male *Col13a1*^{oe} (5, 4, 7, 7, 5), female WT (4, 4, 5, 5, 4), female *Col13a1*^{oe} (6, 4, 6, 7, 6). *q < 0.05, **q < 0.01, and ***q < 0.001 determined by two-way ANOVA followed by FDR.

Figure 3. *Col13a1*^{oe} mice have trabecular bone changes. Representative µCT images of distal trabecular bone of WT and *Col13a1*^{oe} male (A) and female (B) mice femurs; µCT analysis of WT and *Col13a1*^{oe} mice trabecular bone fraction (BV/TV) (C) and trabecular number (Tb.N) (D). Number of mice analyzed ordered by increasing age: male WT (6, 4, 6, 4, 6), male *Col13a1*^{oe} (5, 4, 7, 7, 5), female

WT (4, 4, 5, 5, 4), female *Col13a1*^{oe} (6, 4, 6, 7, 6). *q < 0.05, **q < 0.01, and ***q < 0.001 determined by two-way ANOVA followed by FDR.

Figure 4. Bone composition and morphology is altered in *Col13a1*^{oe} mice. XPS analysis of calcium (A) and nitrogen content (B) of 4- and 25-week-old mouse femurs. Representative SHG images of 12-week-old WT (C) and *Col13a1*^{oe} (D) mouse tibia mid-diaphysis cortical bone. White arrows indicate the direction of ColI fibers, and grey arrows indicate bright ColI signals. Scale bars 10 μm. SEM images of the lacuno-canalicular system via PMMA embedding followed by acid etching of 4-week-old WT (E and G) and *Col13a1*^{oe} (F and H) mouse vertebrae. Scale bars 1 μm E-F and 10 μm G-H. Rhodamine 6G stained longitudinal sections of 4-week-old WT (I) and *Col13a1*^{oe} (J) femurs and maximum intensity projection of cross-sections of 12-week-old WT (K) and *Col13a1*^{oe} (L) femurs. Scale bars 20 μm I-J, 10 μm K-L. IHC staining of VEGF on 4-week-old WT (M) and *Col13a1*^{oe} (N) mouse tibia, scale bars 50 μm. VEGF localizes mainly on the endosteal osteoblasts (red arrows), vessels in the endosteum (black arrowheads), and on the blood vessels inside the cortical bone (black arrow). XPS studies are shown as combined results from both genders: WT male n = 3, female n = 3, *Col13a1*^{oe} male n = 2, female n = 3; SHG imaging n = 3; SEM, rhodamine and VEGF staining n = 3. Representative images are shown. *q < 0.05, **q < 0.01, and ***q < 0.001 determined by two-way ANOVA followed by FDR.

Figure 5. ColXIII overexpression alters osteoblast proliferation, differentiation and matrix production through JNK and ERK signaling pathways. ColXIII (upper) and ColI (lower) WB of primary osteoblasts extracted from femurs of 4-week-old WT and *Col13a1*^{oe} mice (A). IEM images of the matrix produced by primary osteoblast cultured 21 days in osteogenic medium and stained with a

ColI antibody (black dots), scale bars 500 nm, inset 100 nm (B). Calcium content (C) and ALP activity (D) of primary osteoblasts cultured in osteogenic medium. Cell confluence of primary osteoblast at 72 h treated with SP600125, PD184352 (5 μM), Wortmannin (Wort, 1 μM) or an integrin β1-blocking antibody (β1 Ab, 2.5 μg/ml) (E). Number of osteoblasts divided per bone perimeter (N.Ob/B.Pm) of 4-week-old mouse L4 vertebrae (F). MC3T3-E1 osteoblasts treated with *COL13A1*^{oe}-CHO CM for 1 h showed increased pJNK/JNK (G) and pERK/ERK ratios (H). pAkt/Akt is statistically unchanged (I). MC3T3-E1 osteoblasts treated with *COL13A1*^{oe}-CHO CM for 24 h have increased VEGF expression (J). n = 5 calcium and ALP, n = 8 for proliferation; for histomorphometry, male WT n = 6, *Col13a1*^{oe} n = 5, female, WT n = 4, *Col13a1*^{oe} n = 3. *q < 0.05 and ***q < 0.001 determined by two-way ANOVA followed by FDR. n = 6 for WB, *p < 0.05, **p < 0.01, and ***p < 0.001 determined by Student's t-test with Welch's correction.

Figure 6. ColXIII increases angiogenesis in the mouse metatarsal angiogenesis assay. Maximum intensity projections of CD31 (red) staining of WT (A, C, and F) and *Col13a1*^{oe} (B, E, and G) metatarsal assays at culture day 7. Quantitative analysis of angiogenesis of different treatments, SP600125 (5 μM, WT n = 4, *Col13a1*^{oe} n = 5) or integrin β1-blocking antibody (2.5 μg/ml, n = 6), compared with controls (n = 7) and normalized to bone size (C). ColXIII (green) and CD31 (red) staining in WT (H) and *Col13a1*^{oe} (I) metatarsal cultures: dashed lines indicate the borders of metatarsal bone, scale bars 100 μm. *q < 0.05, **q < 0.01, and ***q < 0.001 determined by two-way ANOVA followed by FDR.

Figure 7. *Col13a1*^{oe} osteoblasts boost osteoclast resorption activity. TRAP staining of mouse primary osteoclast treated with conditioned medium (CM) from WT (A) or *Col13a1*^{oe} (B) osteoblasts, scale bars 200 μm. SEM images of resorption pits (arrows) of mouse primary osteoclast treated with CM from WT (C) or *Col13a1*^{oe} (D) osteoblast, scale bar 100 μM. The number of osteoclasts per bone chip after a 7-day culture (E). Resorption percentage per osteoclast (F). n = 6, **q < 0.01 one-way ANOVA followed by FDR.

Figure 8. Schematic representation of key findings. ColXIII activates the ERK and JNK pathways through β1-integrins and upregulates VEGF expression in osteoblasts. In turn, VEGF enhances bone angiogenesis and activates osteoclast resorption activity. Moreover, overexpression of ColXIII disturbs osteoblast differentiation and the development of the lacunar-canalicular network (LCN).

Highlights

Collagen XIII expression is significantly upregulated in mesenchymal stem cells of osteoporotic patients

Overexpression of collagen XIII causes cortical bone deterioration in mice

Enzymatically cleaved collagen XIII ectodomain enhances angiogenesis

Soluble collagen XIII ectodomain activates ERK and JNK signaling in osteoblasts

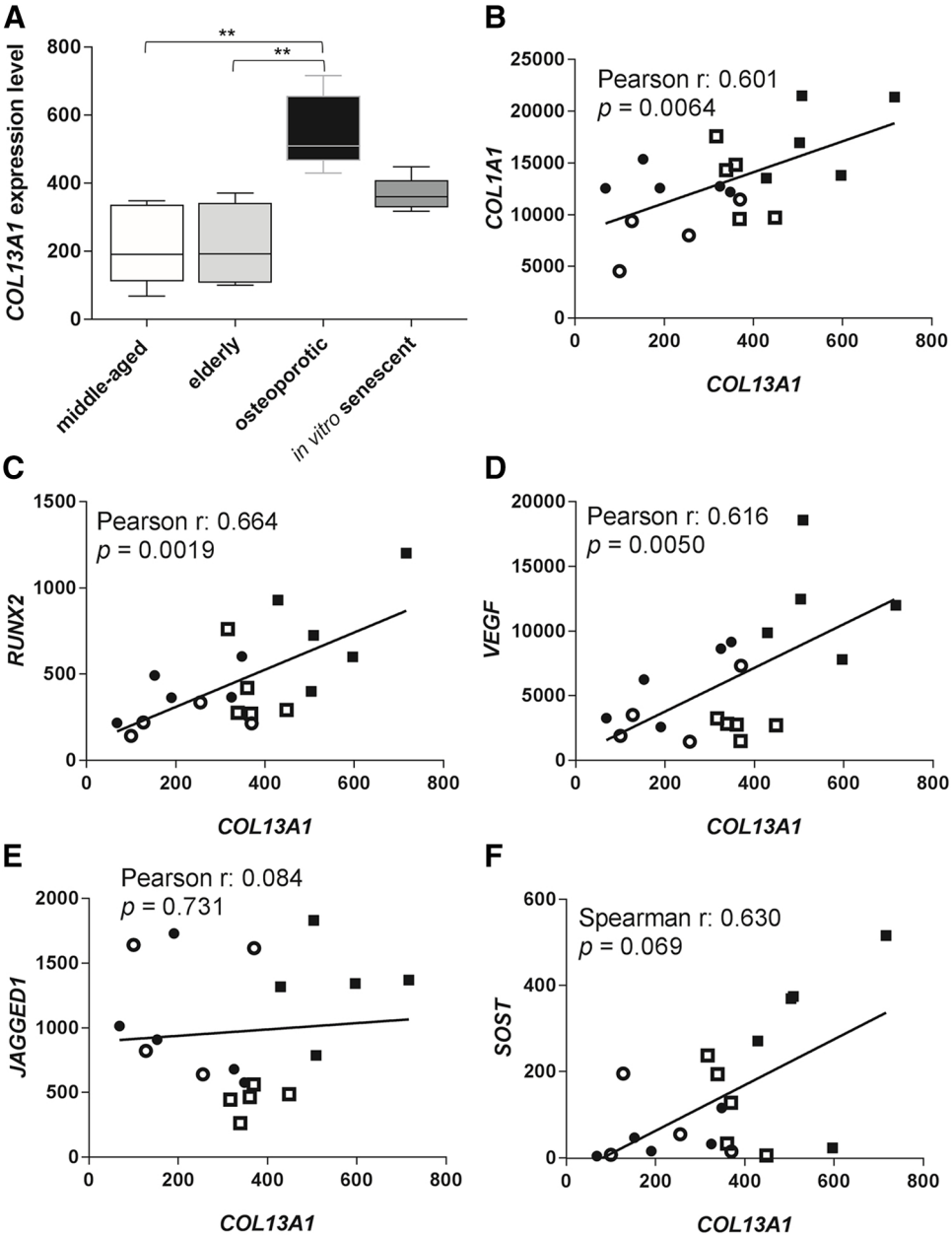
A
COL13A1 expression level
800
600
400
200
0
**
**
middle-aged
elderly
osteoporotic
in vitro senescent
B
Pearson r: 0.601
p = 0.0064
COL1A1
25000
20000
15000
10000
5000
0
200
400
600
800
COL13A1
C
Pearson r: 0.664
p = 0.0019
RUNX2
1500
1000
500
0
200
400
600
800
COL13A1
D
Pearson r: 0.616
p = 0.0050
VEGF
20000
15000
10000
5000
0
200
400
600
800
COL13A1
E
Pearson r: 0.084
p = 0.731
JAGGED1
2000
1500
1000
500
0
200
400
600
800
COL13A1
F
Spearman r: 0.630
p = 0.069
SOST
600
400
200
0
200
400
600
800
COL13A1

Figure 1

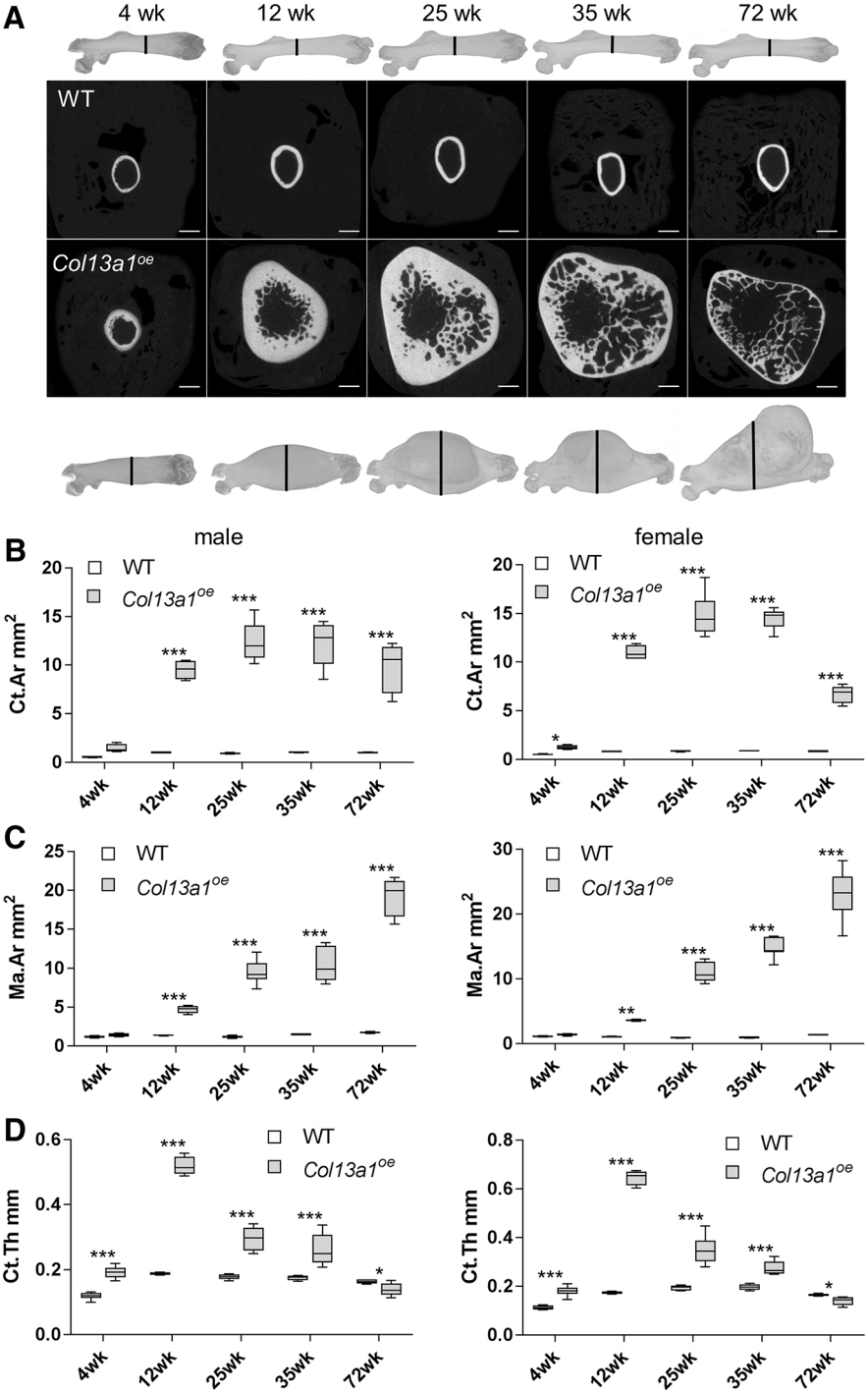
A
4 wk
12 wk
25 wk
35 wk
72 wk
WT
Col13a1oe
B
male
female
WT
Col13a1oe
Ct.Ar mm2
C
Ma.Ar mm2
D
Ct.Th mm
4wk
12wk
25wk
35wk
72wk

Figure 2

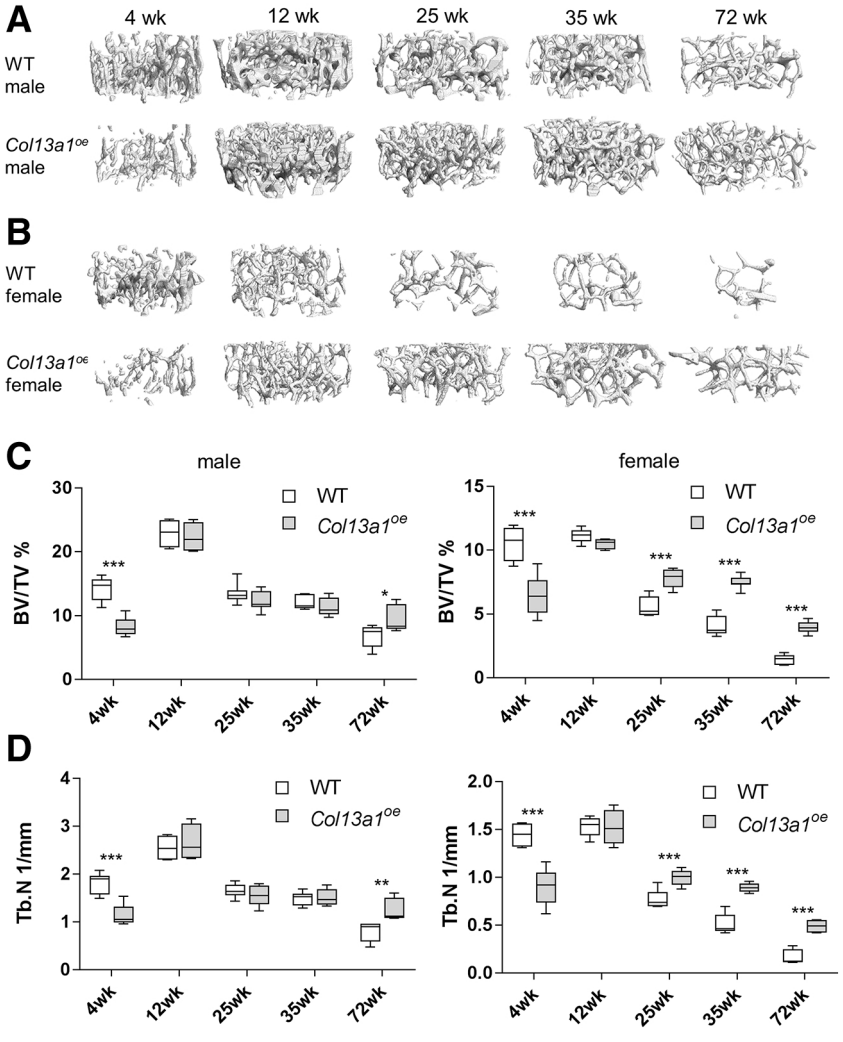
A
4 wk
12 wk
25 wk
35 wk
72 wk
WT male
Col13a1oe male
B
WT female
Col13a1oe female
C
male
female
BV/TV %
WT
Col13a1oe
4wk
12wk
25wk
35wk
72wk
D
Tb.N 1/mm

Figure 3

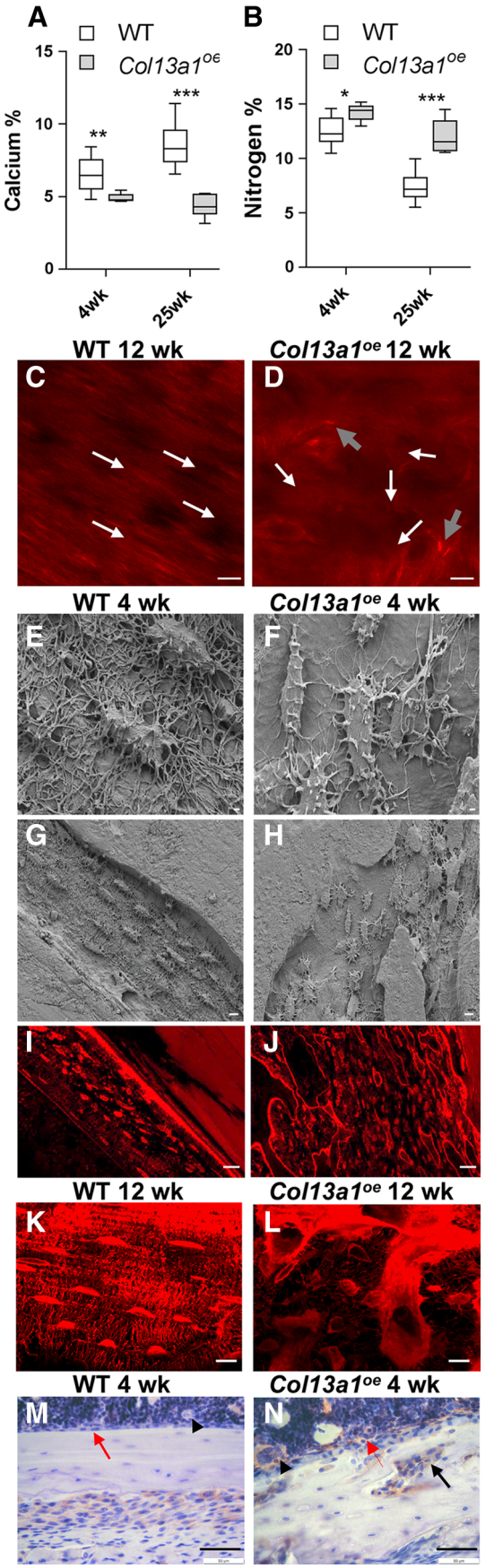
A
WT
Col13a1oe
Calcium %
15
10
5
0
**
***
4wk
25wk
B
WT
Col13a1oe
Nitrogen %
20
15
10
5
0
*
***
4wk
25wk
WT 12 wk
Col13a1oe 12 wk
C
D
WT 4 wk
Col13a1oe 4 wk
E
F
G
H
I
J
WT 12 wk
Col13a1oe 12 wk
K
L
WT 4 wk
Col13a1oe 4 wk
M
N

Figure 4

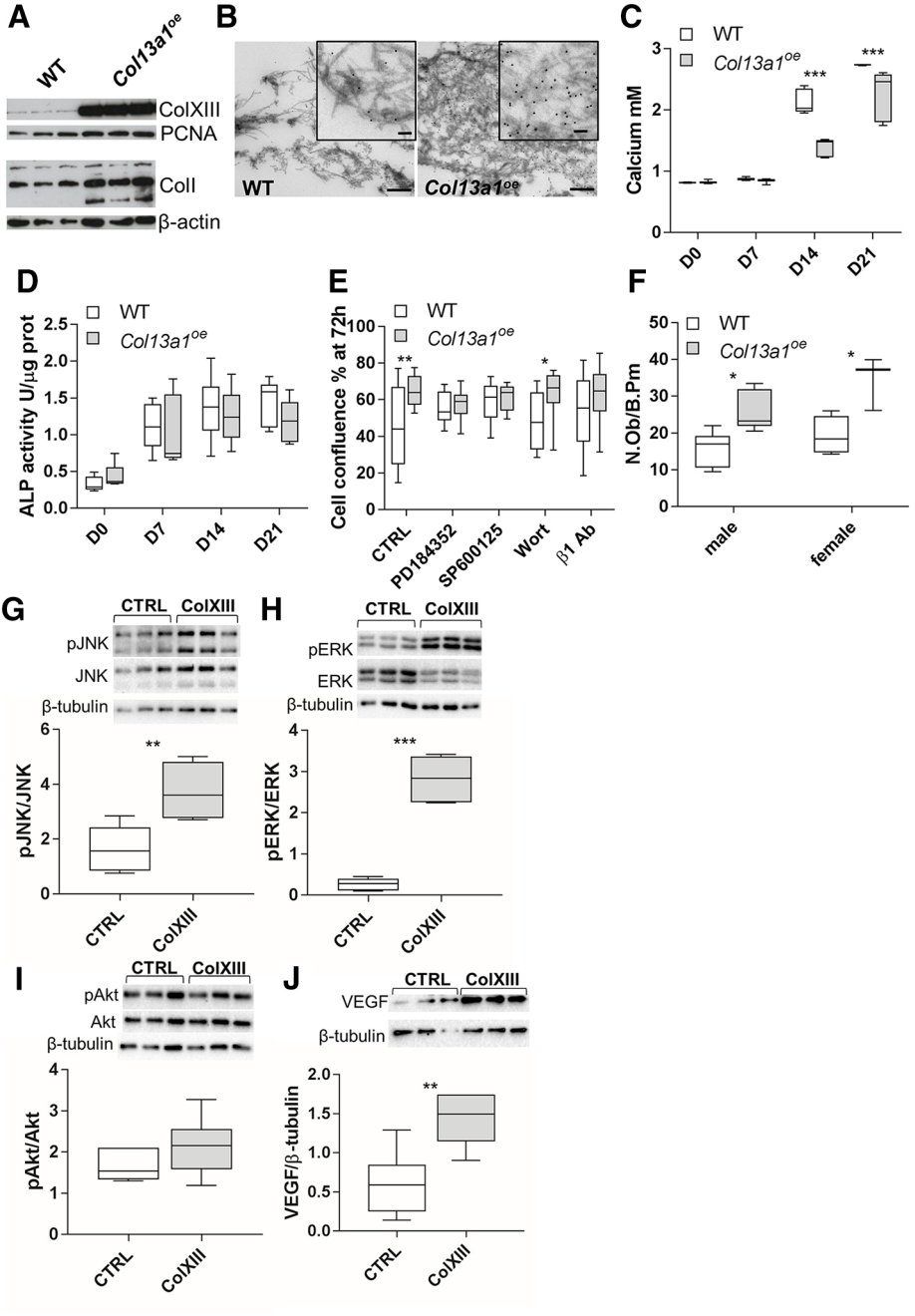
A
WT
Col13a1oe
ColXIII
PCNA
ColI
β-actin
B
WT
Col13a1oe
C
WT
Col13a1oe
Calcium mM
D0
D7
D14
D21
D
WT
Col13a1oe
ALP activity U/μg prot
D0
D7
D14
D21
E
WT
Col13a1oe
Cell confluence % at 72h
CTRL
PD184352
SP600125
Wort
β1 Ab
F
WT
Col13a1oe
N.Ob/B.Pm
male
female
G
CTRL
ColXIII
pJNK
JNK
β-tubulin
pJNK/JNK
H
CTRL
ColXIII
pERK
ERK
β-tubulin
pERK/ERK
I
CTRL
ColXIII
pAkt
Akt
β-tubulin
pAkt/Akt
J
CTRL
ColXIII
VEGF
β-tubulin
VEGF/β-tubulin

Figure 5

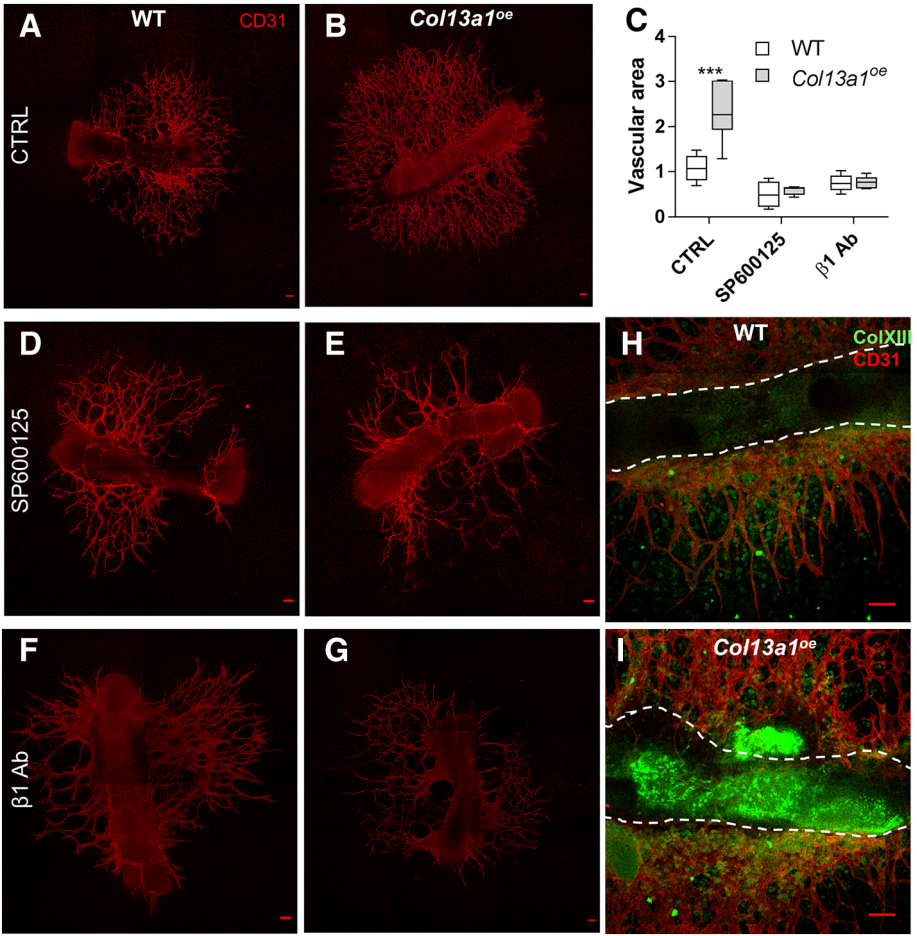
A
WT
CD31
CTRL
B
Col13a1oe
C
Vascular area
WT
Col13a1oe
***
CTRL
SP600125
β1 Ab
D
SP600125
E
H
WT
ColXIII
CD31
F
β1 Ab
G
I
Col13a1oe

Figure 6

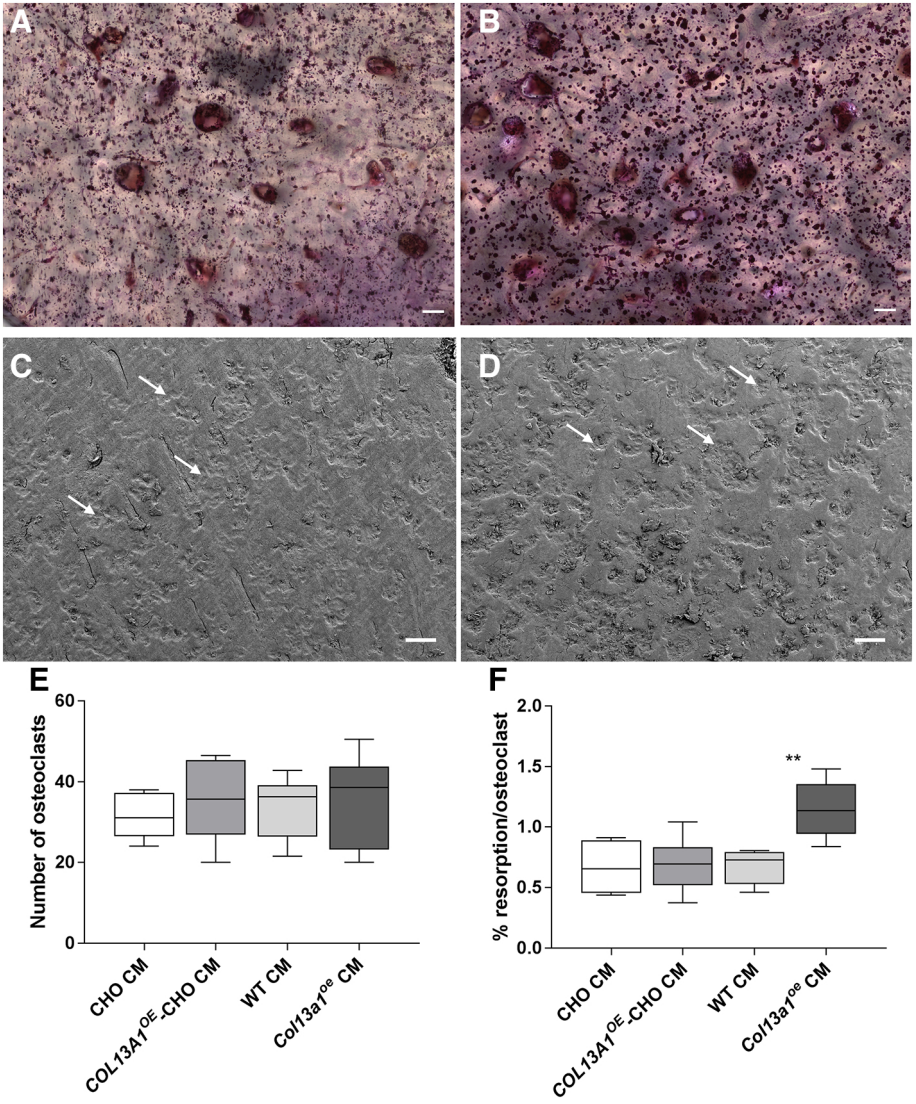
A
B
C
D
E
Number of osteoclasts
60
40
20
0
CHO CM
COL13A1OE-CHO CM
WT CM
Col13a1oe CM
F
% resorption/osteoclast
2.0
1.5
1.0
0.5
0.0
**
CHO CM
COL13A1OE-CHO CM
WT CM
Col13a1oe CM

Figure 7

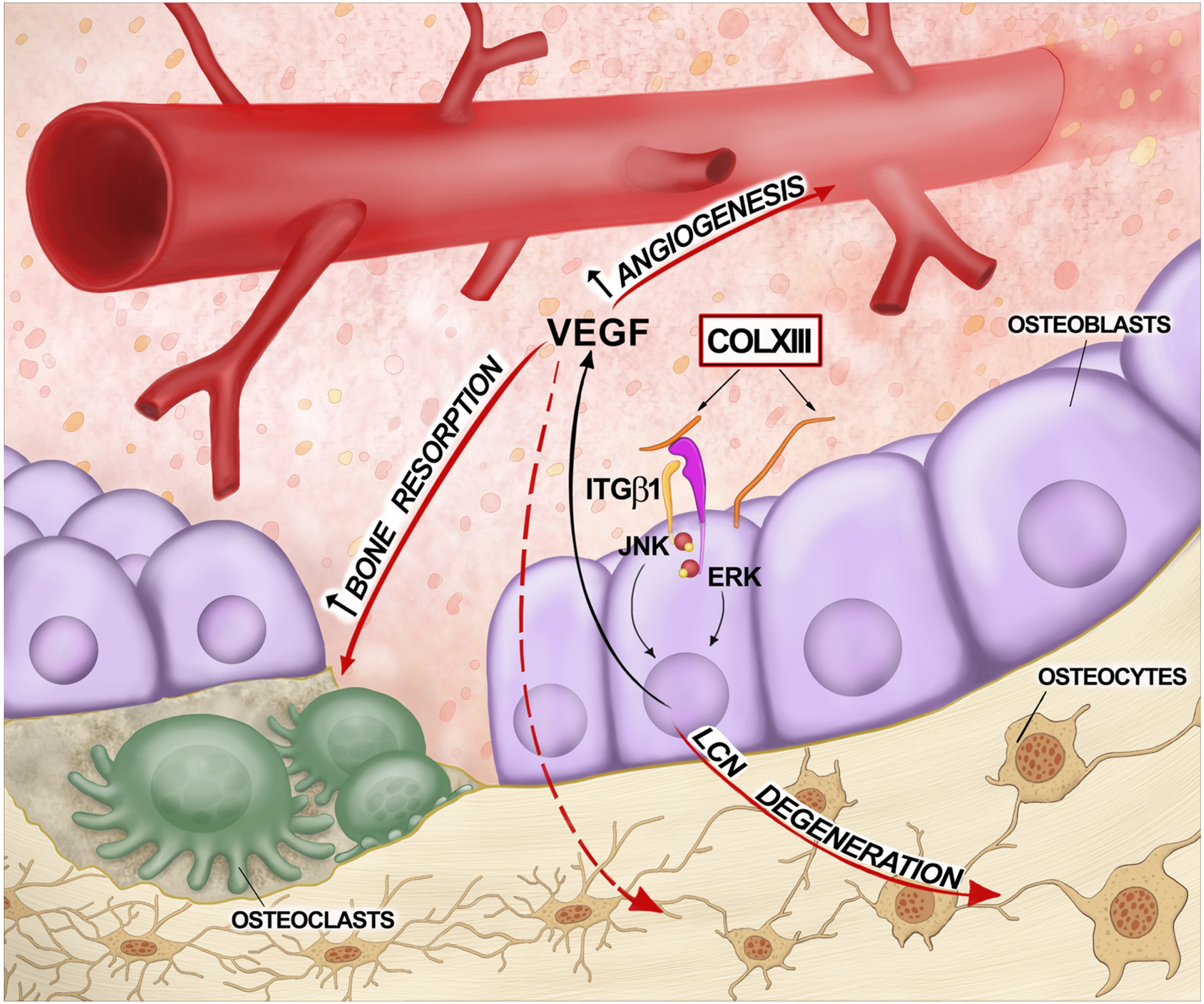
↑ ANGIOGENESIS
VEGF
COLXIII
OSTEOBLASTS
↑ BONE RESORPTION
ITGβ1
JNK
ERK
OSTEOCYTES
LCN DEGENERATION
OSTEOCLASTS

Figure 8